Supporting Information

Generic and Facile Mechanochemical Access to Versatile Lattice-Confined Pd(II)-based Heterometallic Sites

Zhuorigebatu Tegudeer,[a] Jisue Moon,[b] Joshua Wright,[c] Milton Das,[d] Gayan Rubasinghege,[d] Wenqian Xu,[e] and Wen-Yang Gao*[a]

[a]*Department of Chemistry and Biochemistry, Ohio University, Athens, Ohio 45701, United States*
[b]*Chemical Sciences Division, Oak Ridge National Laboratory, Oak Ridge, Tennesse 37831, United States*
[c]*Department of Physics, Illinois Institute of Technology, Chicago, Illinois 60616, United States*
[d]*Department of Chemistry, New Mexico Institute of Mining and Technology, Socorro, New Mexico 87801, United States*
[e]*X-ray Science Division, Advanced Photon Source, Argonne National Laboratory, Lemont, Illinois 60439, United States*

Email: gaow@ohio.edu

Table of Contents

A. General Considerations

Materials Solvents were obtained as ACS reagent grade and used as received. Unless otherwise noted, all chemicals and solvents were used as received. Methanol (MeOH), dichloromethane (CH_2Cl_2), acetic acid (HOAc), acetonitrile (MeCN), ethyl acetate, and hexanes were obtained from VWR Chemicals BDH. 1,3,5-Benzentricarboxylic acid (H_3btc), nickel(II) acetate tetrahydrate ($Ni(OAc)_2{\cdot}4H_2O$), copper(II) acetate monohydrate ($Cu(OAc)_2{\cdot}H_2O$), and palladium(II) acetate ($Pd(OAc)_2$) were obtained from Oakwood Chemical. Manganese acetate tetrahydrate ($Mn(OAc)_2{\cdot}4H_2O$) and formic acid were obtained from Beantown Chemical. Cobalt(II) acetate tetrahydrate ($Co(OAc)_2{\cdot}4H_2O$) was purchased from Chem-Impex Int'l Inc. (*E*)-Hex-4-en-1-ol and 1,3,5-tris(4-carboxyphenyl)benzene were obtained from Ambeed. Zinc acetate dihydrate ($Zn(OAc)_2{\cdot}2H_2O$) and (diacetoxyiodo)benzene ($PhI(OAc)_2$) were obtained from Acros Organics. 3-Phenyl-1-propanol was obtained from Aldrich Chemical Company Inc. Rhodium(II) acetate was obtained from Thermos Scientific. Chlorosulfonyl Isocyanate was obtained from TCI Chemicals. Compounds of *trans*-4-hexenyl sulfamate (**1**),[1] (*E*)-4-(prop-1-en-1-yl)-1,2,3-oxathiazinane 2,2-dioxide (**2**), and 8-methyl-3-oxa-2-thia-1-azabicyclo[5.1.0]octane 2,2-dioxide (**3**)[2] were prepared according to literature methods. UHP-grade N_2 and He, used in gas adsorption measurements, were obtained from Air gas. All reactions were carried out under ambient atmosphere unless otherwise noted.

Mechanochemical Synthesis Mechanochemical synthesis was conducted using a Retsch Mixer Mill MM 400. Starting materials were loaded into a 10 mL Teflon grinding jar with 2 grinding balls (Teflon or stainless steel, 10 mm Ø). Careful attention should be given to the correct loading of the milling cups to the mill before mixing.

Characterization Details Solution-phase UV-vis spectra were recorded by an Agilent Cary 60 UV-vis Spectrophotometer. Diffuse reflectance UV-vis spectra were recorded by Agilent Cary 60 with a remote diffuse reflectance accessory (VideoBarrelino™, a product from Harrick Scientific). Thermogravimetric analysis (TGA) was performed on a Shimadzu DTG-60 analyzer with a ramping rate of 15 °C/min. IR spectra were recorded on a Thermo Nicolet Avatar 370 DTGS spectrometer with a SMART PERFORMER ATR module. Spectra were blanked against air and were determined as the average of 50 scans. IR data are reported as follows: wavenumber (cm^{-1}), (peak intensity: s, strong; m, medium; w, weak). Inductively coupled plasma mass spectrometry (ICP-MS) measurements were carried out on an Agilent Technologies 7900 ICP-MS with an ASX-500 Series autosampler. The solids were digested in conc. HCl or HNO_3 by sonication and diluted with ultrapure water. Gas chromatography (GC) analysis was carried out using a Shimadzu GC-17A.

Gas Sorption Details N_2 adsorption isotherms (0−1.0 bar pressure range) were measured volumetrically at 77 K using a Quantachrome Autosorb-iQ. The sample was transferred under N_2 atmosphere to pre-weighed analysis tubes. The sample was evacuated at 100 °C until the outgas rate was <10 μbar/min and further maintained for 16 h. The tube was weighed to determine the mass of the activated sample. The tube was transferred to the analysis port of the instrument. UHP-grade (99.999% purity) N_2 and He were used for all adsorption measurements. Brunauer-Emmett-Teller (BET) surface areas were calculated in relative pressure range 0.02 to 0.15.

Powder X-ray Diffraction (PXRD) In-house PXRD measurements were carried out on a Panalytical X'Pert Pro Diffractometer (Cu Kα, 1.5418 Å; 45 kV, 40 mA). The angular range was measured from 4.00 to 50.00° (2θ) with steps of 0.017° and a measurement time of 0.4 seconds per step. Synchrotron 2-D PXRD data were collected in capillaries with the sample-to-detector distance at 700 mm and λ = 0.45212 Å at beamline 17-BM of Advanced Photon Source at Argonne National Laboratory. The data were integrated using the software GSAS-II[3] to produce 1-D powder X-ray diffraction patterns. Simulated PXRD patterns were calculated using Mercury.[4]

X-ray Absorption Details X-ray absorption fine structure (EXAFS) data were collected on beamline 10-ID-B (The Materials Research Collaborative Access Team, MRCAT) of the Advanced Photon Source (APS) at Argonne National Laboratory. The solid powder samples were loaded into Nylon plastic washers (ID 9.9mm) using Kapton tape on both ends. The reported spectra were collected in the fluorescence mode, and data sets were collected until the adequate signal to noise was obtained (3 – 6 scans). Metal foils were collected for proper background subtraction.

The data were processed with the Athena and Artemis programs of the IFEFFIT package.[5] Reference foil data were aligned to the first zero-crossing of the second derivative of normalized $\mu(E)$ data, which was calibrated to the literature E_0 value for the K-edge. Spectra were averaged in $\mu(E)$ prior to normalization. Background removal was achieved by spline fitting. EXAFS data were extracted above the threshold energy, E_0. FEFF 6[6] was used to calculate theoretical phases and amplitudes from structure models consisting of crystal structures or the Cartesian coordinates of geometrically optimized computational models. All data were initially fitted with simultaneous k-weighting of 1, 2, and 3, then finalized with k^3-weighting in R-space. Fit windows in k-space were determined based on the lowest quality data collected. Cu, Pd, and Co data sets were from 1.0 to 10.0 $Å^{-1}$ (k-space) and 1.0 to 4.0 Å (R-space). Structural parameters that were determined by the fit include the reduction factor (S_0^2), the bond distance (R), the mean squared relative displacement of the scattering element (σ^2), and the energy shift of the photoelectron(ΔE_0).

B. Synthesis and Characterization

Synthesis of $[PdCu(OAc)_4(OH_2)]\cdot(HOAc)_2$

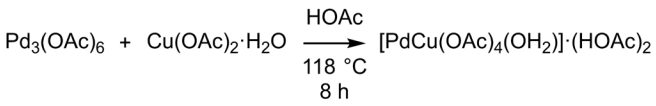

This synthetic procedure was adapted from the literature.[7] A 10-mL round bottom flask was charged with 2 Teflon grinding balls, $Pd_3(OAc)_6$ (0.100 g, 0.148 mmol, 1.00 equiv), $Cu(OAc)_2\cdot H_2O$ (0.087 g, 0.44 mmol, 3.0 equiv), and acetic acid (HOAc, 3.0 mL). The reaction mixture was stirred at 118 °C for 8 h. The reaction mixture was cooled to 23 °C and then kept in a refrigerator at 4 °C for 6 h. The precipitated crystals of $[PdCu(OAc)_4(OH_2)]\cdot(HOAc)_2$ were collected by filtration and were dried at 23 °C to afford yellow solids (0.104 g, 44% yield). The solids were characterized by PXRD (Figure S1), well matched to the calculated ones. UV-vis spectrum (Figure S6, HOAc): λ_{max} (nm, $\varepsilon(M^{-1}cm^{-1})$): 355 (890). IR (Figure S7, cm^{-1}): 1602(m), 1511(s), 1424(s), 1352(w), 1044(w), 1032(w), 696(s). Spectral data are well-matched with those available in the literature.[7] Solid-state UV-vis diffuse reflectance spectrum: Figure S15.

Synthesis of $[PdZn(OAc)_4(OH_2)]\cdot(HOAc)_2$

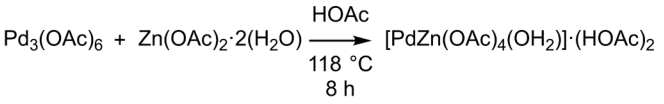

This synthetic procedure was adapted from the literature.[7] A 10-mL round bottom flask was charged with 2 Teflon grinding balls, $Pd_3(OAc)_6$ (0.100 g, 0.148 mmol, 1.00 equiv), $Zn(OAc)_2\cdot 2H_2O$ (0.098 g, 0.44 mmol, 3.0 equiv), and acetic acid (HOAc, 3.0 mL). The reaction mixture was stirred at 118 °C for 8 h. The reaction mixture was cooled to 23 °C and then kept in a refrigerator at 4 °C for 6 h. The precipitated crystals of $[PdZn(OAc)_4(OH_2)]\cdot(HOAc)_2$ were collected by filtration and were dried at 23 °C to afford light orange solids (0.215 g, 90% yield). The solids were characterized by PXRD (Figure S2), well matched to the calculated ones. UV-vis spectrum (Figure S6, HOAc): λ_{max} (nm, $\varepsilon(M^{-1}cm^{-1})$): 337 (1800). IR (Figure S7, cm^{-1}): 1702(m), 1616(s), 1517(w), 1507(w), 1410(s), 1394(s), 1345(m), 1336(m), 1263(m), 1049(w), 1027(w), 889(w), 699(s). Spectral data are well-matched with those available in the literature.[7] Solid-state UV-vis diffuse reflectance spectrum: Figure S28a.

Synthesis of $[PdCo(OAc)_4(OH_2)]\cdot(HOAc)_2$

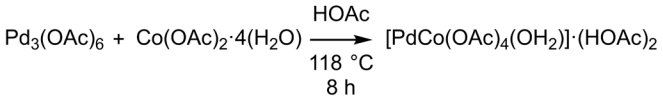

This synthetic procedure was adapted from the literature.[7] A 10-mL round bottom flask was charged with 2 Teflon grinding balls, $Pd_3(OAc)_6$ (0.100 g, 0.148 mmol, 1.00 equiv), $Co(OAc)_2\cdot4H_2O$ (0.111 g, 0.444 mmol, 3.00 equiv), and acetic acid (HOAc, 3.0 mL). The reaction mixture was stirred at 118 °C for 8 h. The reaction mixture was cooled to 23 °C and then kept in a refrigerator at 4 °C for 6 h. The precipitated crystals of $[PdCo(OAc)_4(OH_2)]\cdot(HOAc)_2$ were collected by filtration and were dried at 23 °C to afford brown solids (0.209 g, 87% yield). The solids were characterized by PXRD (Figure S3), well matched to the calculated ones. UV-vis spectrum (Figure S6, HOAc): λ_{max} (nm, $\varepsilon(M^{-1}cm^{-1})$): 334 (2400). IR (Figure S7, cm^{-1}): 1703(m), 1601(s), 1428(m), 1387(s), 1346(m), 1333(m), 1264(m), 1048(w), 1026(w), 888(w), 698(s). Spectral data are well-matched with those available in the literature.[7] Solid-state UV-vis diffuse reflectance spectrum: Figure S28b.

Synthesis of $[PdMn(OAc)_4(OH_2)]\cdot(HOAc)_2$

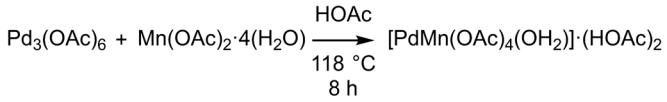

This synthetic procedure was adapted from the literature.[7] A 10-mL round bottom flask was charged with 2 Teflon grinding balls, $Pd_3(OAc)_6$ (0.100 g, 0.148 mmol, 1.00 equiv), $Mn(OAc)_2\cdot4H_2O$ (0.109 g, 0.444 mmol, 3.00 equiv), and acetic acid (HOAc, 2.0 mL). The reaction mixture was stirred at 118 °C for 8 h. The reaction mixture was cooled to 23 °C and then kept in a refrigerator at 4 °C for 6 h. The precipitated crystals of $[PdMn(OAc)_4(OH_2)]\cdot(HOAc)_2$ were collected by filtration and were dried at 23 °C to afford orange solids (0.126 g, 63% yield). The solids were characterized by PXRD (Figure S4), well matched to the calculated ones. UV-vis spectrum (Figure S6, HOAc): λ_{max} (nm, $\varepsilon(M^{-1}cm^{-1})$): 340 (910). IR (Figure S7, cm^{-1}): 1760(w), 1731(w), 1710(w), 1618(s), 1558(w), 1445(w), 1410(m), 1391(m), 1341(m), 1240(w). 1029(w), 698(s). Spectral data are well-matched with those available in the literature.[7] Solid-state UV-vis diffuse reflectance spectrum: Figure S28c.

Synthesis of $[PdNi(OAc)_4(OH_2)]\cdot(HOAc)_2$

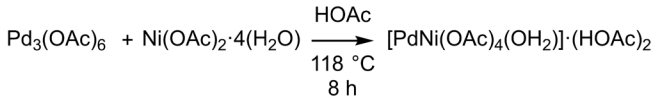

This synthetic procedure was adapted from the literature.[7] A 10-mL round bottom flask was charged with 2 Teflon grinding balls, $Pd_3(OAc)_6$ (0.100 g, 0.148 mmol, 1.00 equiv), $Ni(OAc)_2\cdot4H_2O$ (0.111 g, 0.444 mmol, 3.00 equiv), and acetic acid (HOAc, 3.0 mL). The reaction mixture was stirred at 118 °C for 8 h. The reaction mixture was cooled to 23 °C and then kept in a refrigerator at 4 °C for 6 h. The precipitated crystals of $[PdNi(OAc)_4(OH_2)]\cdot(HOAc)_2$ were collected by filtration and were dried at 23 °C to afford dark yellow solids (0.184 g, 77% yield). The solids were characterized by PXRD (Figure S5), well matched to the calculated ones. UV-vis spectrum (Figure S6, HOAc): λ_{max} (nm, $\varepsilon(M^{-1}cm^{-1})$): 328 (2100). IR (Figure S7, cm^{-1}): 1708(s), 1616(s), 1600(s), 1429(w), 1395(s), 1382(m), 1364(w), 1341(m), 1334(w), 1257(s), 1050(w), 1023(w), 702(s). Spectral data are well-matched with those available in the literature.[7] Solid-state UV-vis diffuse reflectance spectrum: Figure S28d.

Mechanochemical Synthesis of $[(PdCu)_3(btc)_4]$

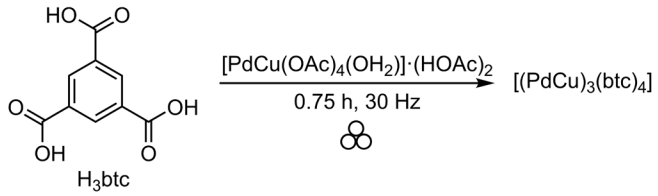

A 10-mL Teflon grinding jar was charged with $[PdCu(OAc)_4(OH_2)]\cdot(HOAc)_2$ (0.038 g, 0.070 mmol, 1.0 equiv), 1,3,5-benzenetricarboxylic acid (H_3btc, 0.020 g, 0.095 mmol, 1.4 equiv), EtOH (35 μL, η = 0.60 μL/mg), and 2 Teflon grinding balls. The resulting mixture was milled using a Retsch Mixer Mill MM 400 at 30 Hz for 0.75 h. After the milling, a characteristic odor of HOAc was smelled. The obtained product was collected and washed with acetone (10 mL × 3). The solids were dried under reduced pressure to afford the compound, $[(PdCu)_3(btc)_4]$ (0.031 g, 98% yield) as a dark green colored solid. Primary data are presented in the following figures: PXRD data, Figures 3a, S8 and S9; XANES, Figures 4a and S10; EXAFS, Figures 4b and S11–S12, Tables S1 and S2; IR spectrum, Figure S13; TGA plot, Figure S14; 77 K N_2 adsorption isotherm, Figure 3b; ICP-MS data, Table S3; UV-vis diffusion reflectance spectrum, Figure S15; IR, Figure S16.

Mechanochemical Synthesis of $[(PdZn)_3(btc)_4]$

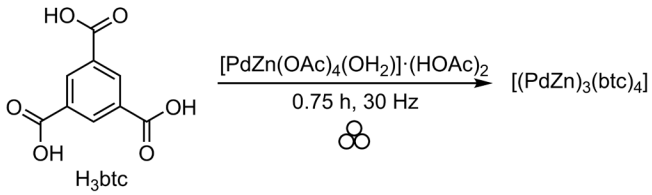

A 10-mL Teflon grinding jar was charged with $[PdZn(OAc)_4(OH_2)]\cdot(HOAc)_2$ (0.038 g, 0.070 mmol, 1.0 equiv), 1,3,5-benzenetricarboxylic acid (H_3btc, 0.020 g, 0.095 mmol, 1.4 equiv), EtOH (52 μL, η = 0.90 μL/mg), and 2 Teflon grinding balls. The resulting mixture was milled using a Retsch Mixer Mill MM 400 at 30 Hz for 0.75 h. After the milling, a characteristic odor of HOAc was smelled. The obtained product was collected and washed with acetone (10 mL × 3). The solids were dried under reduced pressure to afford the compound, $[(PdZn)_3(btc)_4]$ (0.031 g, 98% yield) as a light brown colored solid. Primary data are presented in the following figures: PXRD data, Figures 3a; IR spectrum, Figure S16; 77 K N_2 adsorption isotherm, Figure S17 and Table S4; ICP-MS data, Table S3; EXAFS, Figures S18 and S20; XANES, Figure S19; UV-vis diffusion reflectance spectrum, Figure S28a.

Mechanochemical Synthesis of $[(PdMn)_3(btc)_4]$

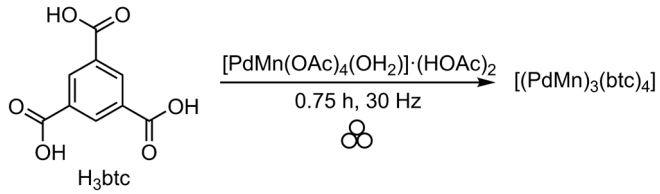

A 10-mL Teflon grinding jar was charged with $[PdMn(OAc)_4(OH_2)]\cdot(HOAc)_2$ (0.038 g, 0.071 mmol, 1.0 equiv), 1,3,5-benzenetricarboxylic acid (H_3btc, 0.020 g, 0.095 mmol, 1.3 equiv), EtOH (52 μL, η = 0.90 μL/mg), and 2 Teflon grinding balls. The resulting mixture was milled using a Retsch Mixer Mill MM 400 at 30 Hz for 0.75 h. After the milling, a characteristic odor of HOAc was smelled. The obtained product was collected and washed with acetone (10 mL × 3). The solids were dried under reduced pressure to afford the title compound, $[(PdMn)_3(btc)_4]$ (0.030 g, 97% yield) as a brown colored solid. Primary data are presented in the following figures: PXRD data, Figures 3a; IR spectrum, Figure S16; 77 K N_2 adsorption isotherm, Figure S17 and Table S4; ICP-MS data, Table S3; EXAFS, Figures S18 and S22; XANES, Figure S21; UV-vis diffusion reflectance spectrum, Figure S28c.

Mechanochemical Synthesis of $[(PdCo)_3(btc)_4]$

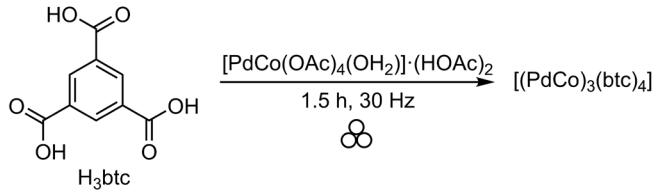

A 10-mL Teflon grinding jar was charged with $[PdCo(OAc)_4(OH_2)]\cdot(HOAc)_2$ (0.038 g, 0.070 mmol, 1.0 equiv), 1,3,5-benzenetricarboxylic acid (H_3btc, 0.020 g, 0.095 mmol, 1.4 equiv), EtOH (52 μL, η = 0.90 μL/mg), and 2 Teflon grinding balls. The resulting mixture was milled using a Retsch Mixer Mill MM 400 at 30 Hz for 1.5 h. After the milling, a characteristic odor of HOAc was smelled. The obtained product was collected and washed with acetone (10 mL × 3). The solids were dried under reduced pressure to afford the compound, $[(PdCo)_3(btc)_4]$ (0.030 g, 97% yield) as a dark brown colored solid. Primary data are presented in the following figures: PXRD data, Figures 3a; IR spectrum, Figure S16; 77 K N_2 adsorption isotherm, Figure S17 and Table S4; ICP-MS data, Table S3; XANES, Figure S23; EXAFS, Figures S24, and S25, Tables S5 and S6; UV-vis diffusion reflectance spectrum, Figure S28b.

Mechanochemical Synthesis of $[(PdNi)_3(btc)_4]$

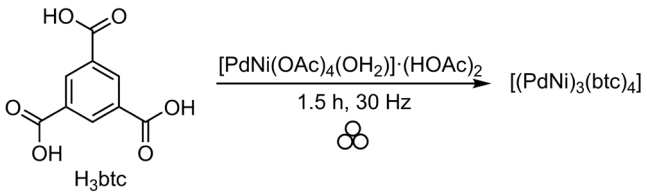

A 10-mL Teflon grinding jar was charged with $[PdNi(OAc)_4(OH_2)]\cdot(HOAc)_2$ (0.038 g, 0.070 mmol, 1.0 equiv), 1,3,5-benzenetricarboxylic acid (H_3btc, 0.020 g, 0.095 mmol, 1.4 equiv), EtOH (52 μL, η = 0.90 μL/mg), and 2 Teflon grinding balls. The resulting mixture was milled using a Retsch Mixer Mill MM 400 at 30 Hz for 1.5 h. After the milling, a characteristic odor of HOAc was smelled. The obtained product was collected and washed with acetone (10 mL × 3). The solids were dried under reduced pressure to afford the title compound, $[(PdNi)_3(btc)_4]$ (0.030 g, 97% yield) as a yellow colored solid. Primary data are presented in the following figures: PXRD data, Figures 3a; IR spectrum, Figure S16; 77 K N_2 adsorption isotherm, Figure S17 and Table S4; ICP-MS data, Table S3; EXAFS, Figures S18 and S27; XANES, Figure S26; UV-vis diffusion reflectance spectrum, Figure S28d.

Mechanochemical Synthesis of $[(PdCu)_3(btb)_4]$

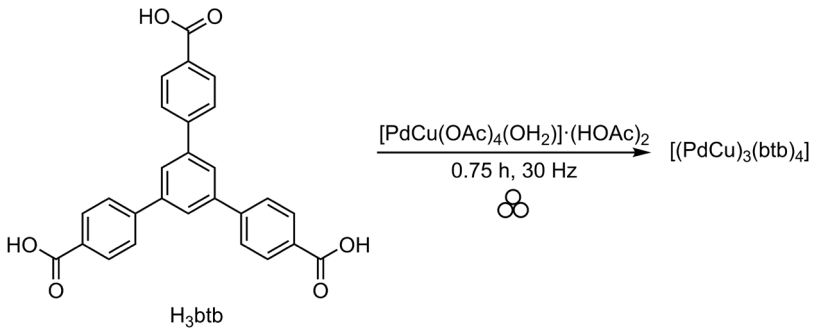

A 10-mL Teflon grinding jar was charged with $[PdCu(OAc)_4(OH_2)]\cdot(HOAc)_2$ (0.033 g, 0.061 mmol, 1.0 equiv), 1,3,5-tris(4-carboxyphenyl)benzene (H_3btb, 0.035 g, 0.080 mmol, 1.3 equiv), EtOH (61 μL, η = 0.90 μL/mg), and 2 Teflon grinding balls. The resulting mixture was milled using a Retsch Mixer Mill MM 400 at 30 Hz for 0.75 h. After the milling, a characteristic odor of HOAc was smelled. The obtained product was collected and washed with acetone (10 mL × 3). The solids were dried under reduced pressure to afford the title compound, $[(PdCu)_3(btb)_4]$ (0.039 g, 98% yield) as a green colored solid. Primary data are presented in the following figures: PXRD data Figure 5; IR spectrum, Figure S29; TGA plot, Figure S30; 77 K N_2 adsorption isotherm, Figure S31.

Mechanochemical Synthesis of $[(PdZn)_3(btb)_4]$

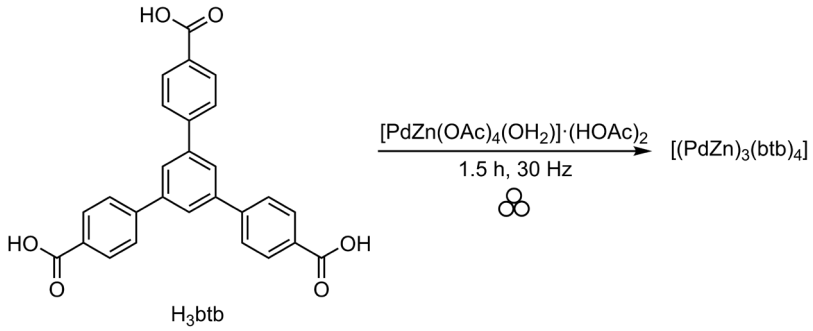

A 10-mL Teflon grinding jar was charged with $[PdZn(OAc)_4(OH_2)]\cdot(HOAc)_2$ (0.033 g, 0.061 mmol, 1.0 equiv), 1,3,5-tris(4-carboxyphenyl)benzene (H_3btb, 0.035 g, 0.080 mmol, 1.3 equiv), EtOH (95 μL, η = 1.4 μL/mg), and 2 Teflon grinding balls. The resulting mixture was milled using a Retsch Mixer Mill MM 400 at 30 Hz for 1.5 h. After the milling, a characteristic odor of HOAc was smelled. The obtained product was collected and washed with acetone (10 mL × 3). The solids were dried under reduced pressure to afford the title compound, $[(PdZn)_3(btb)_4]$ (0.025 g, 62% yield) as a dark brown colored solid. Primary data are presented in the following figures: PXRD data Figure 5; IR spectrum, Figure S29; 77 K N_2 adsorption isotherm, Figure S34.

Mechanochemical Synthesis of $[(PdMn)_3(btb)_4]$

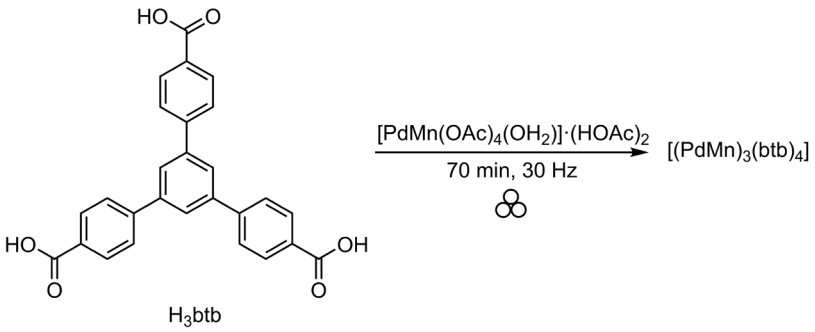

A 10-mL Teflon grinding jar was charged with $[PdMn(OAc)_4(OH_2)]\cdot(HOAc)_2$ (0.033 g, 0.061 mmol, 1.0 equiv), 1,3,5-tris(4-carboxyphenyl)benzene (H_3btb, 0.035 g, 0.080 mmol, 1.3 equiv), EtOH (95 μL, η = 1.4 μL/mg), and 2 Teflon grinding balls. The resulting mixture was milled using a Retsch Mixer Mill MM 400 at 30 Hz for 70 min. After the milling, a characteristic odor of HOAc was smelled. The obtained product was collected and washed with acetone (10 mL × 3). The solids were dried under reduced pressure to afford the title compound, $[(PdMn)_3(btb)_4]$ (0.030 g, 76% yield) as a brown colored solid. Primary data are presented in the following figures: PXRD data Figure 5; IR spectrum, Figure S29; 77 K N_2 adsorption isotherm, Figure S33.

Mechanochemical Synthesis of $[(PdCo)_3(btb)_4]$

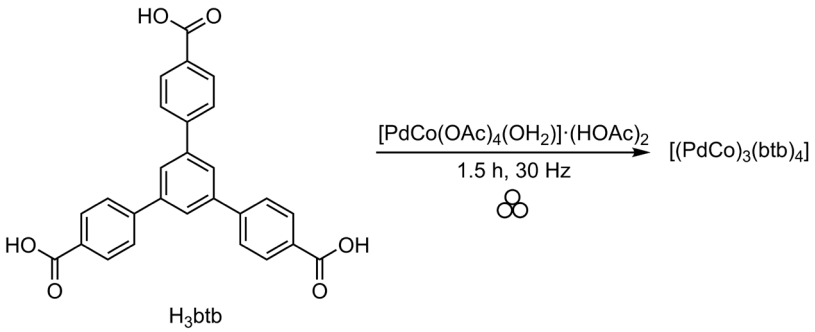

A 10-mL Teflon grinding jar was charged with $[PdCo(OAc)_4(OH_2)]\cdot(HOAc)_2$ (0.033 g, 0.061 mmol, 1.0 equiv), 1,3,5-tris(4-carboxyphenyl)benzene (H_3btb, 0.035 g, 0.080 mmol, 1.3 equiv), EtOH (102 μL, η = 1.5 μL/mg), and 2 stainless steel grinding balls. The resulting mixture was milled using a Retsch Mixer Mill MM 400 at 30 Hz for 1.5 h. After the milling, a characteristic odor of HOAc was smelled. The obtained product was collected and washed with acetone (10 mL × 3). The solids were dried under reduced pressure to afford the title compound, $[(PdCo)_3(btb)_4]$ (0.035 g, 88% yield) as a dark brown colored solid. Primary data are presented in the following figures: PXRD data Figure 5; IR spectrum, Figure S29; 77 K N_2 adsorption isotherm, Figure S32.

C. Supporting Data

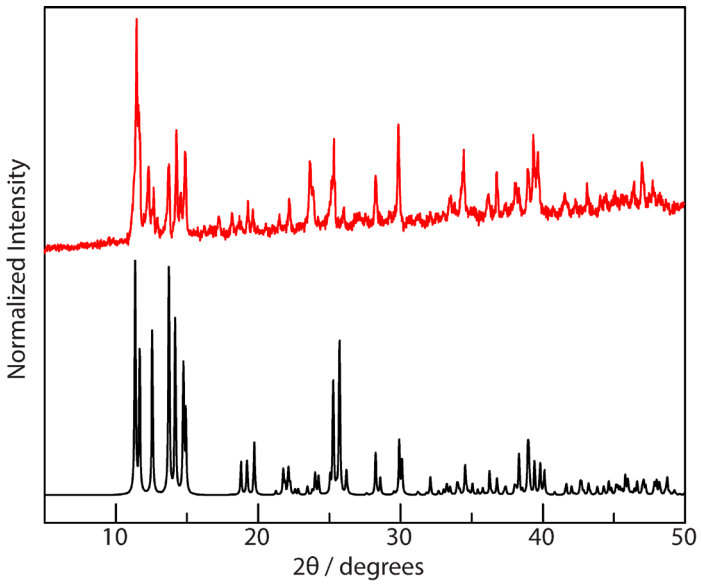

Figure S1. PXRD patterns (λ = 1.5418 Å) of the calculated $[PdCu(OAc)_4(OH_2)]\cdot(HOAc)_2$ (—) are compared with those of the as-synthesized one (—). The displayed patterns indicate the phase purity of the obtained molecular complex.

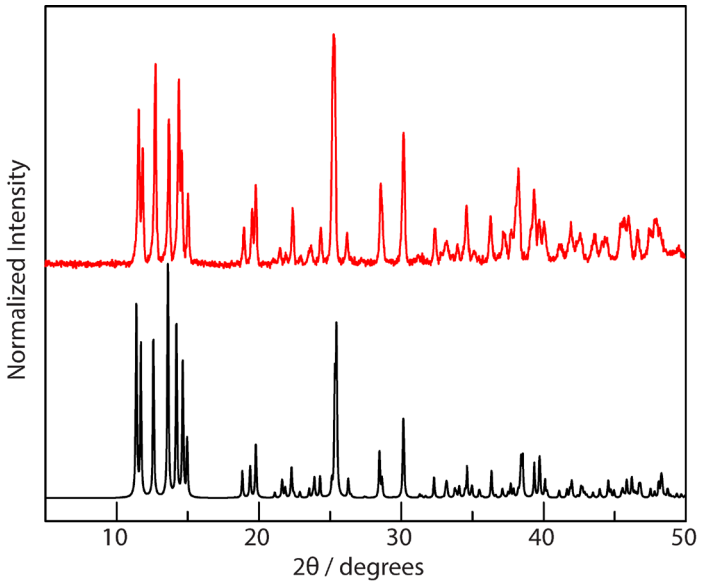

Figure S2. PXRD patterns (λ = 1.5418 Å) of the calculated $[PdZn(OAc)_4(OH_2)]\cdot(HOAc)_2$ (—) are compared with those of the as-synthesized one (—). The displayed patterns indicate the phase purity of the obtained molecular complex.

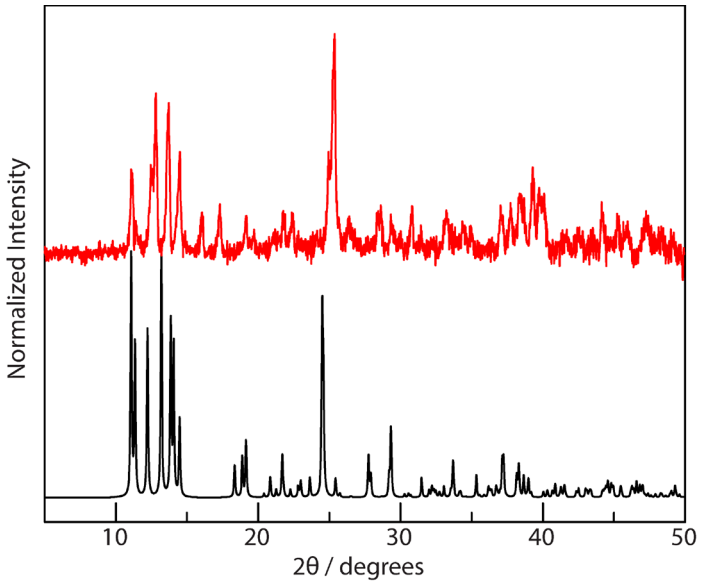

Figure S3. PXRD patterns (λ = 1.5418 Å) of the calculated $[PdCo(OAc)_4(OH_2)]\cdot(HOAc)_2$ (—) are compared with those of the as-synthesized one (—). The displayed patterns indicate the phase purity of the obtained molecular complex.

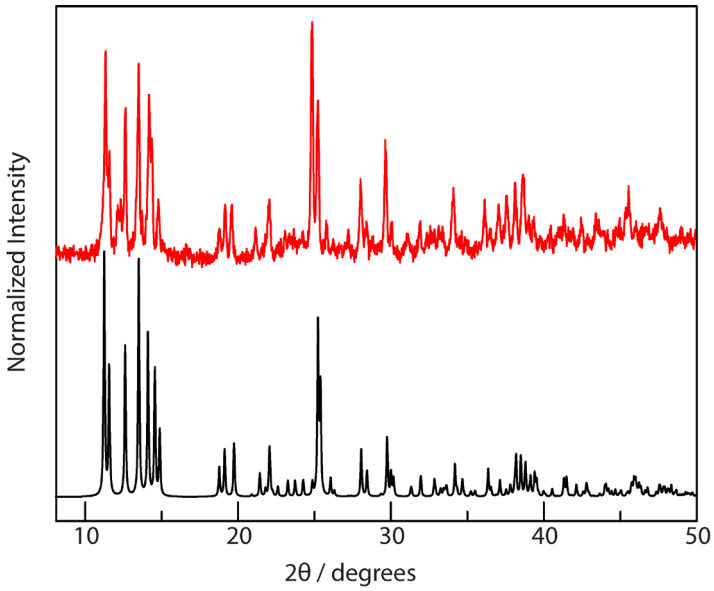

Figure S4. PXRD patterns (λ = 1.5418 Å) of the calculated $[PdMn(OAc)_4(OH_2)]\cdot(HOAc)_2$ (—) are compared with those of the as-synthesized one (—). The displayed patterns indicate the phase purity of the obtained molecular complex.

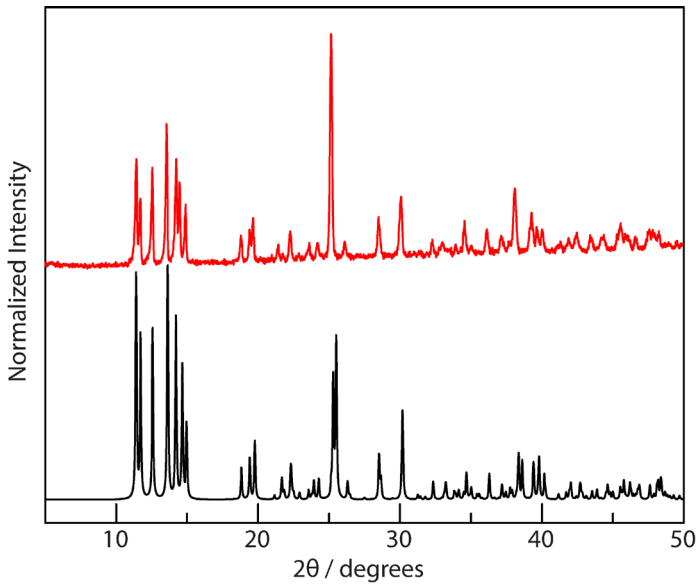

Figure S5. PXRD patterns (λ = 1.5418 Å) of the calculated $[PdNi(OAc)_4(OH_2)]\cdot(HOAc)_2$ (—) are compared with those of the as-synthesized one (—). The displayed patterns indicate the phase purity of the obtained molecular complex.

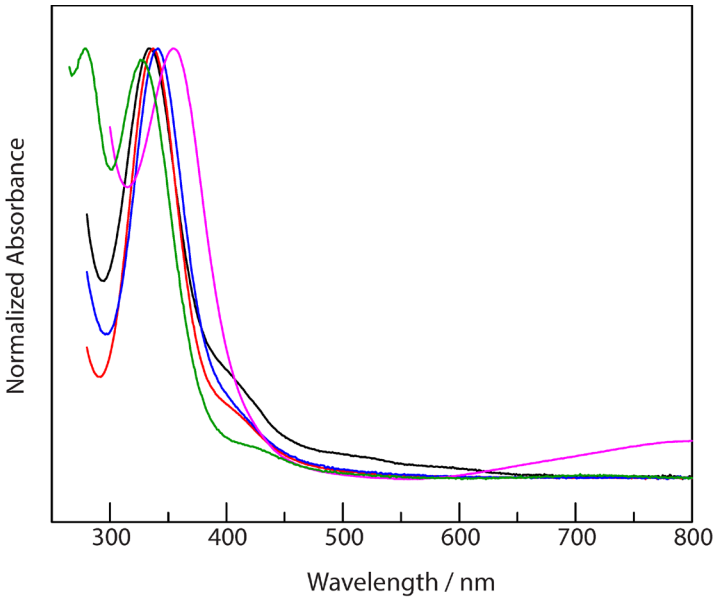

Figure S6. Solution-based UV-vis spectra of molecular complexes $PdCu(OAc)_4$ (—), $PdCo(OAc)_4$ (—), $PdZn(OAc)_4$ (—), $PdMn(OAc)_4$ (—), and $PdNi(OAc)_4$ (—).

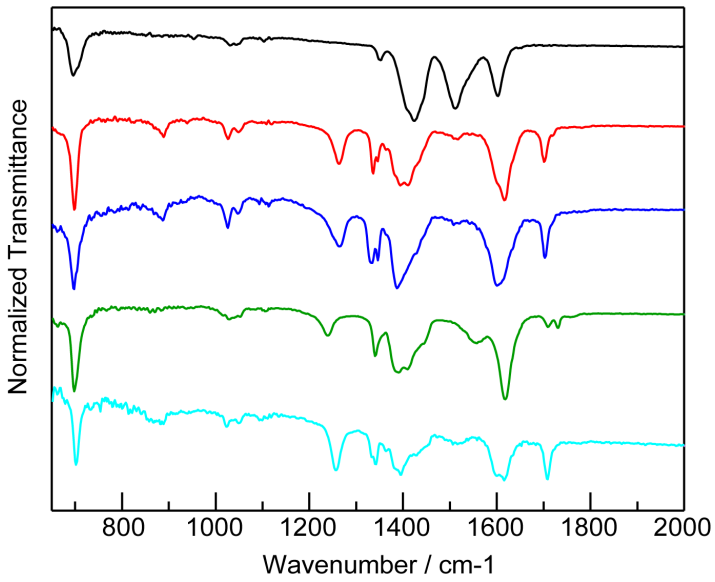

Figure S7. IR spectra (2000–650 cm^{-1}) of molecular complexes $PdCu(OAc)_4$ (—), $PdZn(OAc)_4$ (—), $PdCo(OAc)_4$ (—), $PdMn(OAc)_4$ (—), and $PdNi(OAc)_4$ (—).

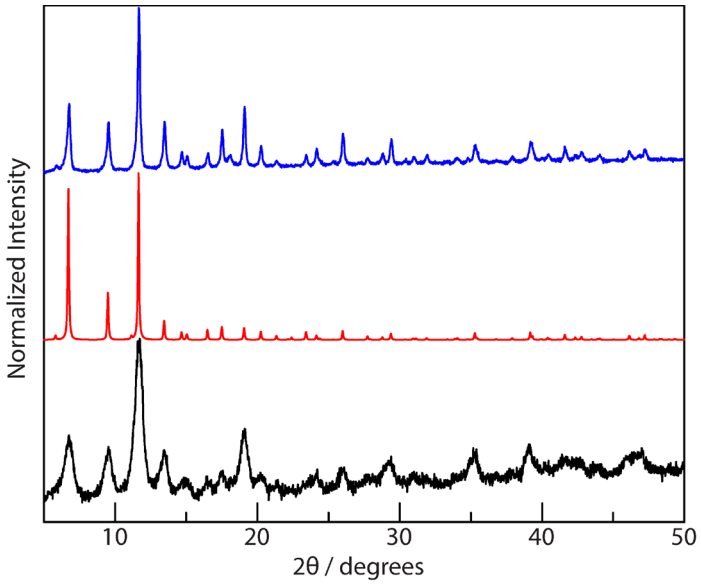

Figure S8. PXRD patterns (λ = 1.5418 Å) of the mechanochemically synthesized $[(PdCu)_3(btc)_4]$ (—), the calculated isostructural $[Cu_3(btc)_2]$ (—), and the mechanochemical synthesized $[Cu_3(btc)_2]$ (—) obtained by milling a 3:2 mixture of $Cu(OAc)_2{\cdot}H_2O$ and H_3btc in the presence of EtOH (η = 0.41 μL/mg, 30 Hz, 0.75 h).

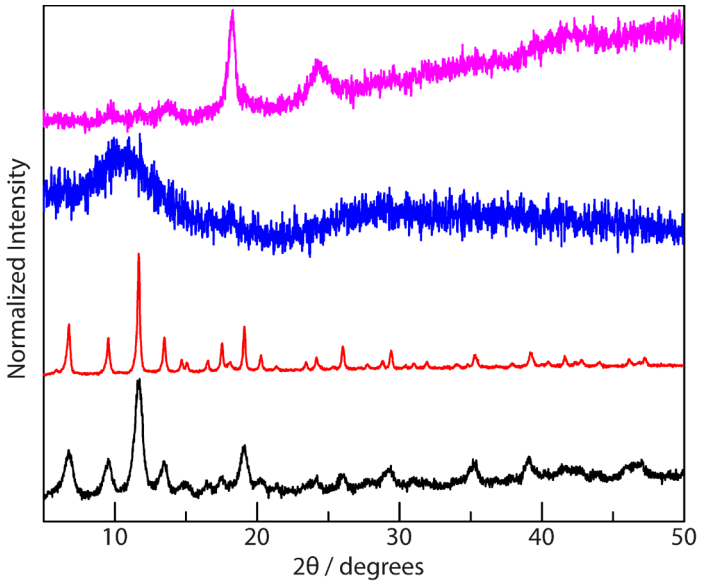

Figure S9. PXRD patterns (λ = 1.5418 Å) of the mechanochemically synthesized $[(PdCu)_3(btc)_4]$ (—), the mechanochemically synthesized isostructural $[Cu_3(btc)_2]$ (—), the amorphous solids (—) obtained by milling $Pd(OAc)_2$ and H_3btc in the presence of EtOH (η = 0.60 μL/mg), and the undesired solids (—) obtained by milling $PdCu(OAc)_4$ and H_3btc under neat conditions without any solvents.

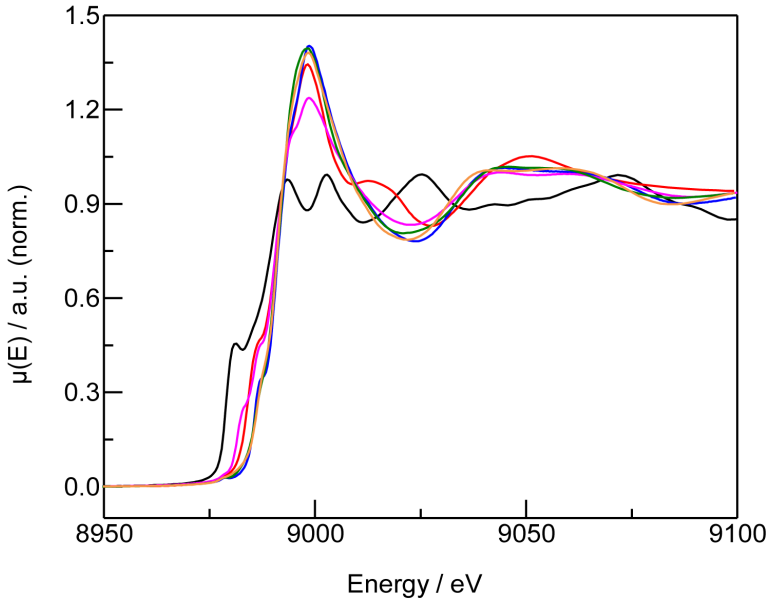

Figure S10. Cu K-edge XANES spectra of Cu(0) foil (—), CuO (—), $[Cu_3(btc)_2]$ (—), $Cu(OAc)_2{\cdot}H_2O$ (—), $PdCu(OAc)_4(OH_2)$ (—) and $[(PdCu)_3(btc)_4]$ (—). These spectra highlight a common Cu(II) oxidation state is observed in $[(PdCu)_3(btc)_4]$, $PdCu(OAc)_4(OH_2)$, $[Cu_3(btc)_2]$, $Cu(OAc)_2{\cdot}H_2O$, CuO, a significant departure from Cu(0).

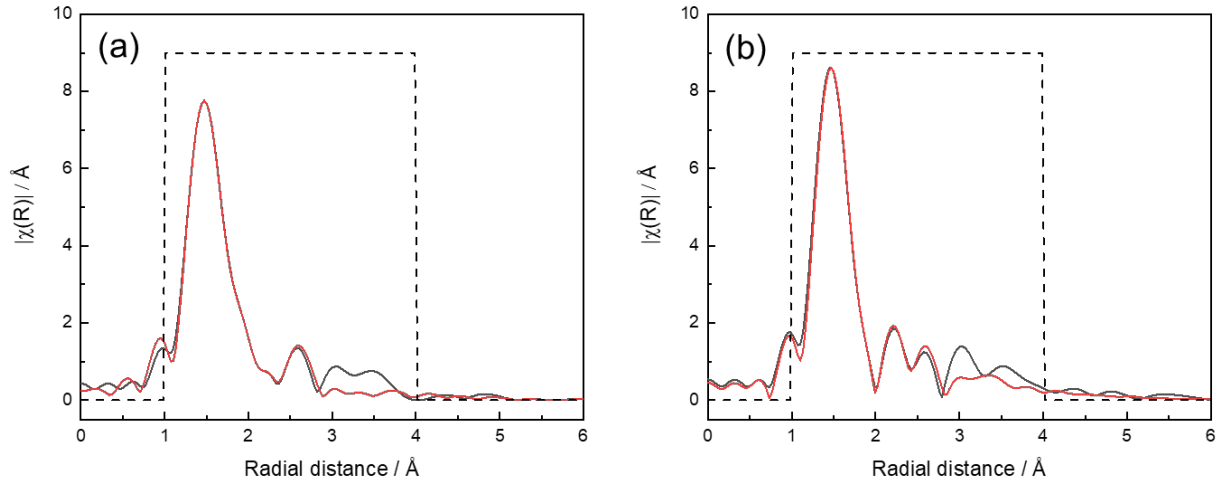

Figure S11. Pd K-edge EXAFS data (fitting range 1.0–4.0 Å) in *R*-space for the $PdCu(OAc)_4(OH_2)$ (a) and $[(PdCu)_3(btc)_4]$ (b) (experimental data (—) and fit (—)).

Table S1. Pd K-edge EXAFS fitting results of $PdCu(OAc)_4(OH_2)$ and $[(PdCu)_3(btc)_4]$.

	Path	R / Å	CN	σ^2 / Å^2	S_0^2	ΔE / eV	R-Factor
$PdCu(OAc)_4(OH_2)$	Pd-O	1.86(1)	2.0	0.004(1)	0.9 ± 0.1	3.08 ± 1	0.014
	Pd-O	2.41(1)	2.0	0.001(3)			
	Pd-Cu	2.99(1)	1.0	0.006(1)			
$[(PdCu)_3(btc)_4]$	Pd-O	1.90(1)	2.0	0.008(2)	0.9 ± 0.1	1.65 ± 1	0.029
	Pd-O	2.36(1)	2.0	0.002(3)			
	Pd-Cu	2.83(1)	1.0	0.003(1)			

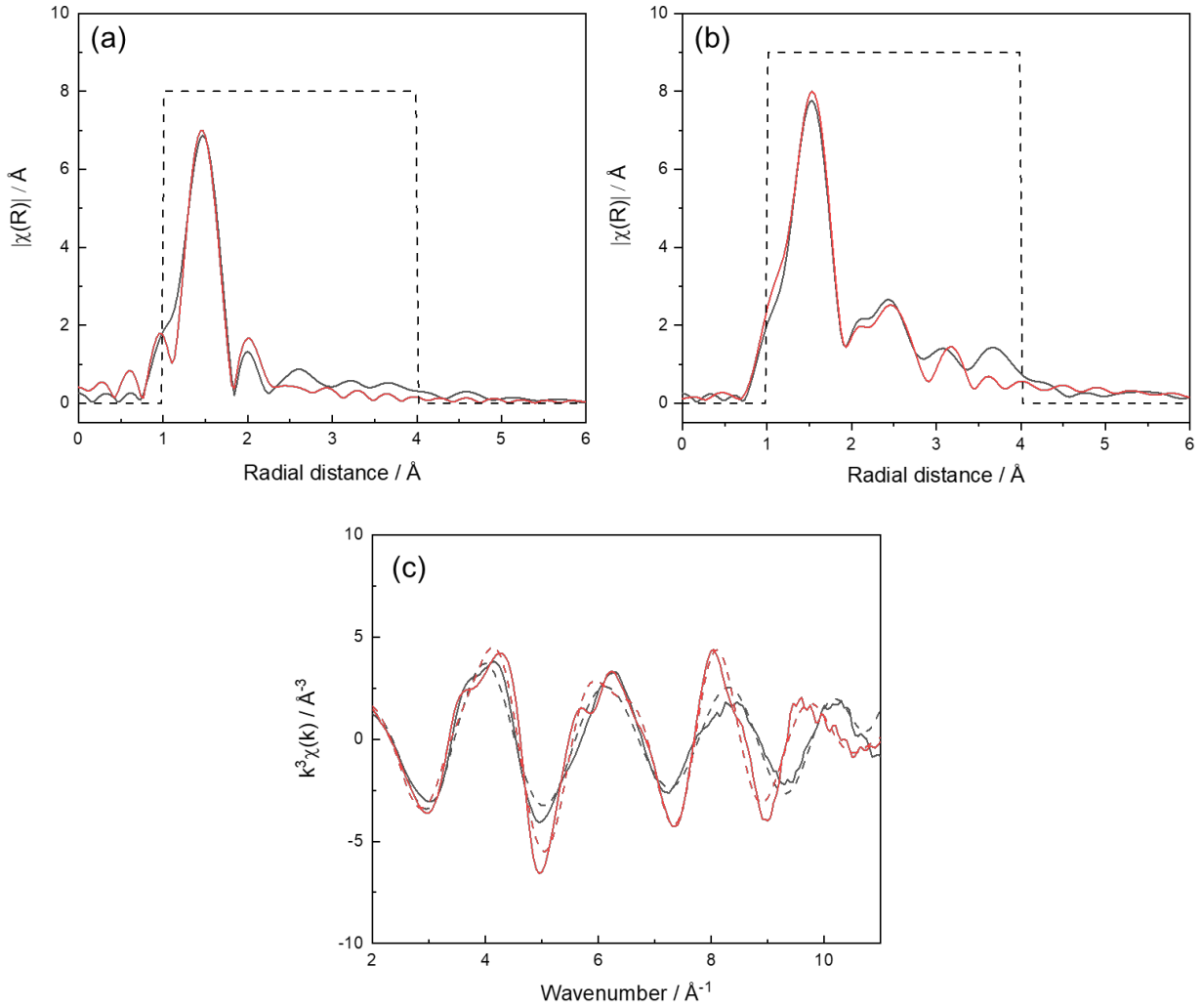

Figure S12. Cu K-edge EXAFS data (fitting range 1.0–4.0 Å) in *R*-space for the $PdCu(OAc)_4(OH_2)$(a) and $[(PdCu)_3(btc)_4]$(b) (experimental data (—) and fit (—)). (c) Cu K-edge EXAFS data (fitting range 1.0–10.0 $Å^{-1}$) in *k*-space for $PdCu(OAc)_4(OH_2)$ (experimental data (—) and fit (----)) and $[(PdCu)_3(btc)_4]$ (experimental data (—) and fit (----)).

Table S2. Cu K-edge EXAFS fitting results of $PdCu(OAc)_4(OH_2)$ and $[(PdCu)_3(btc)_4]$.

	Path	R / Å	CN	σ^2 / Å^2	S_0^2	ΔE / eV	R-Factor
$PdCu(OAc)_4(OH_2)$	Cu-O	1.95(1)	2.0	0.005(2)	0.9 ± 0.1	5.48 ± 1	0.032
	Cu-O	2.09(1)	2.0	0.004(2)			
	Cu-O	2.12(1)	1.0	0.001(1)			
	Cu-Pd	2.46(1)	1.0	0.002(1)			
$[(PdCu)_3(btc)_4]$	Cu-O	1.91(1)	2.0	0.002(2)	0.9 ± 0.1	3.08 ± 1	0.034
	Cu-O	2.07(1)	2.0	0.005(2)			
	Cu-O	2.10(1)	1.0	0.003(1)			
	Cu-Pd	2.43(1)	1.0	0.002(1)			

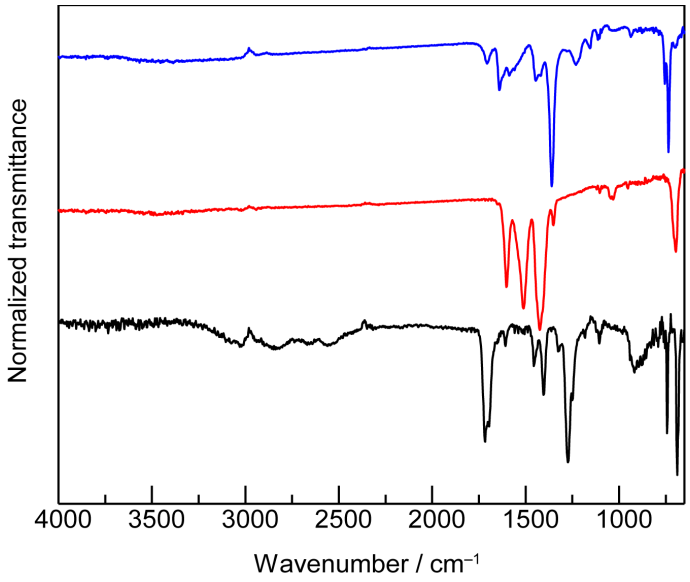

Figure S13. IR spectra (4000–650 cm^{-1}) of H_3btc (—), $PdCu(OAc)_4(OH_2)$ (—), and $[(PdCu)_3(btc)_4]$ (—). IR provides a diagnostic probe for the reaction progress of the mechanochemical synthesis by examining the disappearances of the carbonyl C=O stretch around 1720 cm^{-1} and C–O stretch at 1273 cm^{-1} from carboxylic acid. Furthermore, The incomplete disappearances of the carbonyl C=O stretch and C–O stretch from free carboxylic acid is likely caused by some defects encountered in the solid-state synthesis.

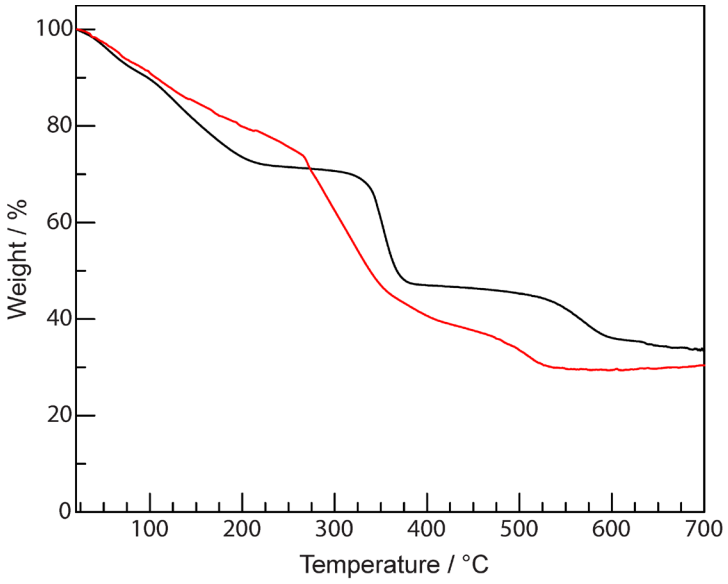

Figure S14. Plots of weight% vs. temperature were obtained by thermogravimetric analysis of $[(PdCu)_3(btc)_4]$ (—) and $[Cu_3(btc)_2]$ (—).

Table S3. The metal ratio of Pd and M (M = Cu, Zn, Mn, Co, and Ni) observed in the mechanochemically prepared $[(PdM)_3(btc)_4]$ materials detected by ICP-MS.

Entry	Pd : M
$[(PdCu)_3(btc)_4]$	1 : 1.06
$[(PdZn)_3(btc)_4]$	1 : 1.01
$[(PdMn)_3(btc)_4]$	1 : 0.82
$[(PdCo)_3(btc)_4]$	1 : 1.02
$[(PdNi)_3(btc)_4]$	1 : 0.92

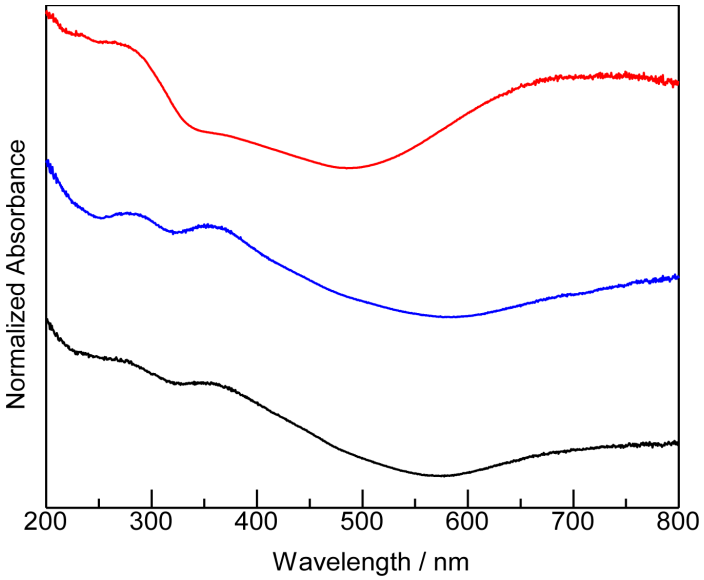

Figure S15. Diffuse reflectance spectra were collected from solid-state $PdCu(OAc)_4$(—), $[(PdCu)_3(btc)_4]$(—), and $[Cu_3(btc)_2]$(—).

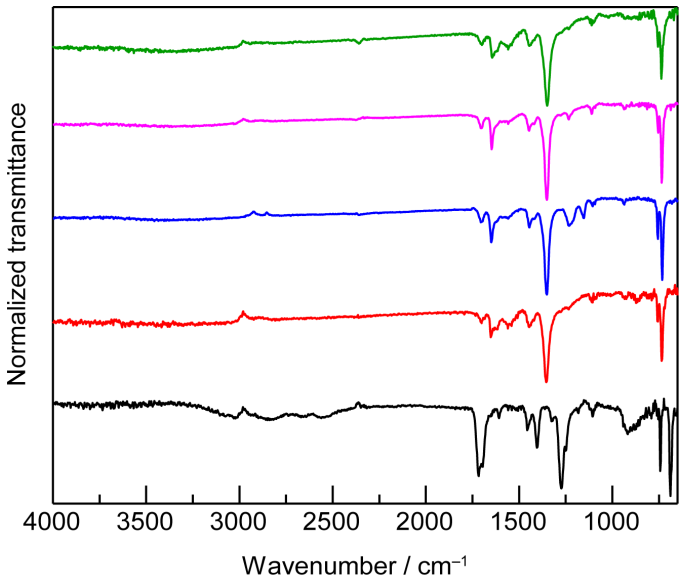

Figure S16. IR spectra (4000–650 cm^{-1}) of H_3btc (—), $[(PdZn)_3(btc)_4]$ (—), $[(PdMn)_3(btc)_4]$ (—), $[(PdCo)_3(btc)_4]$ (—), and $[(PdNi)_3(btc)_4]$ (—). IR provides a diagnostic probe for the reaction progress of mechanochemical synthesis by examining the disappearances of the carbonyl C=O stretch around 1720 cm^{-1} and C–O stretch at 1273 cm^{-1} from initial carboxylic acid. Furthermore, The incomplete disappearances of the carbonyl C=O stretch and C–O stretch from free carboxylic acid is likely caused by some defects encountered in the solid-state synthesis.

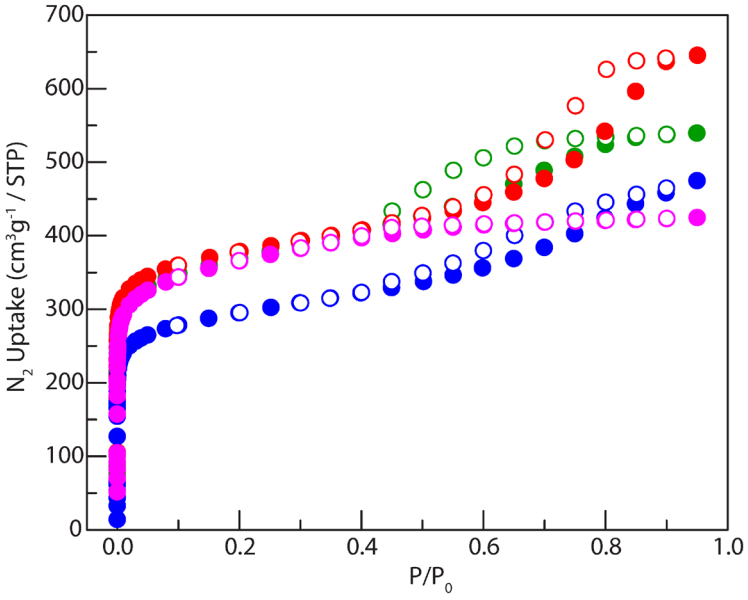

Figure S17. N_2 adsorption isotherms of the mechanochemically obtained $[(PdCo)_3(btc)_4]$ (adsorption (●), desorption (○)), $[(PdMn)_3(btc)_4]$ (adsorption (●), desorption (○)), $[(PdZn)_3(btc)_4]$ (adsorption (●), desorption (○)), and $[(PdNi)_3(btc)_4]$ (adsorption (●), desorption (○)) collected at 77 K.

Table S4. Surface area values of the mechanochemically obtained $[Cu_3(btc)_2]$ and $[(PdM)_3(btc)_4]$ MOFs (M = Cu, Co, Mn, Zn, and Ni) derived from N_2 adsorption isotherms at 77K.

	Brunauer-Emmett-Teller (BET) surface area / m^2/g (P/P_0 = 0.02–0.15)
$[Cu_3(btc)_2]$	1518
$[(PdCu)_3(btc)_4]$	1517
$[(PdCo)_3(btc)_4]$	1369
$[(PdMn)_3(btc)_4]$	1068
$[(PdZn)_3(btc)_4]$	1332
$[(PdNi)_3(btc)_4]$	1321

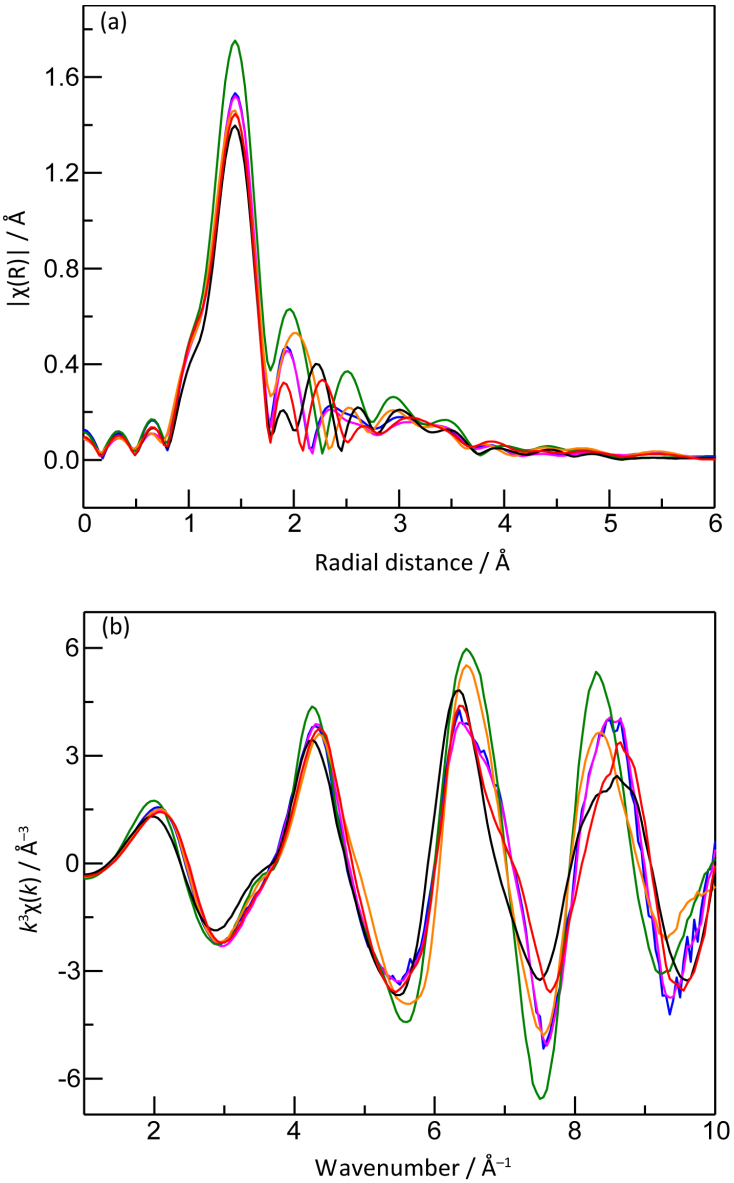

Figure S18. Pd K-edge EXAFS data in *R*-space for $PdZn(OAc)_4(OH_2)$ (—), $[(PdZn)_3(btc)_4]$ (—),$PdMn(OAc)_4(OH_2)$ (—), $[(PdMn)_3(btc)_4]$ (—), $PdNi(OAc)_4(OH_2)$ (—), and $[(PdNi)_3(btc)_4]$ (—). (b) Pd K-edge EXAFS data in *k*-space for $PdZn(OAc)_4(OH_2)$ (—), $[(PdZn)_3(btc)_4]$ (—),$PdMn(OAc)_4(OH_2)$ (—), $[(PdMn)_3(btc)_4]$ (—), $PdNi(OAc)_4(OH_2)$ (—), and $[(PdNi)_3(btc)_4]$ (—). These data highlight that Pd(II) in all the samples shares the same primary coordination sphere and the mechanochemical process does not alternate its primary coordination sphere.

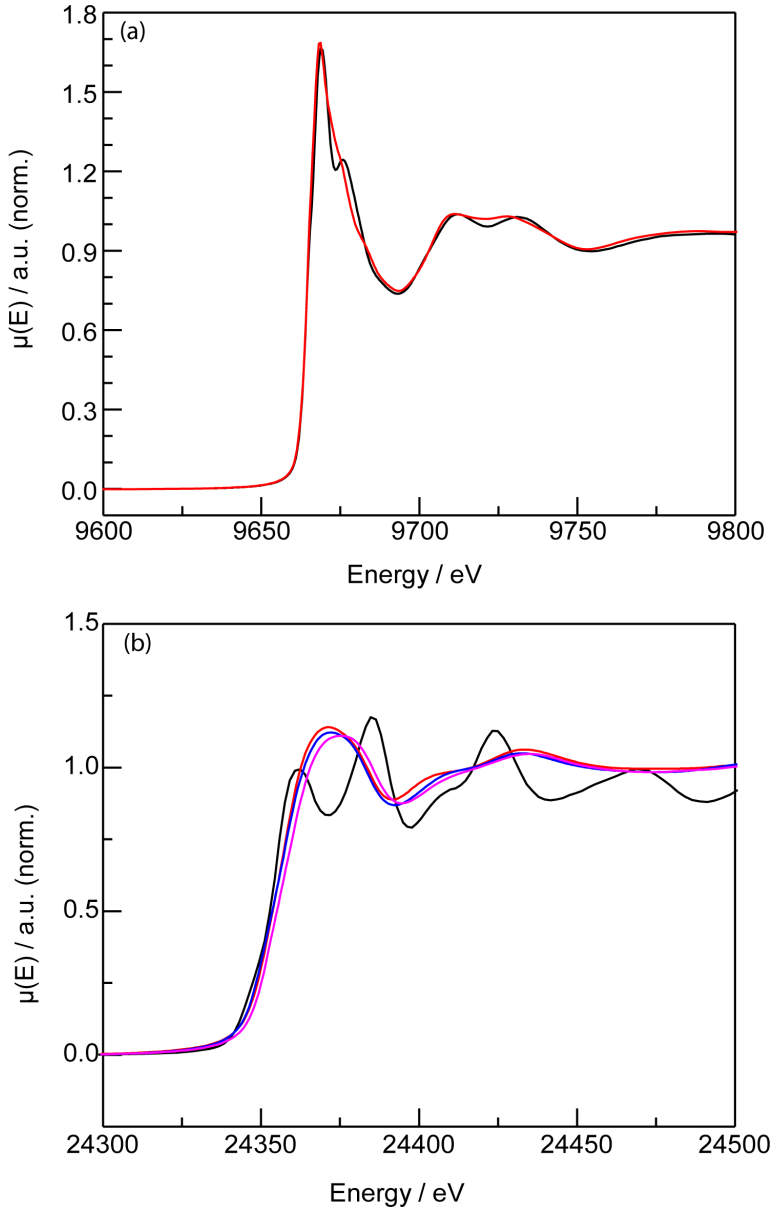

Figure S19. (a) Zn K-edge XANES data collected on for $PdZn(OAc)_4(OH_2)$ (—) and $[(PdZn)_3(btc)_4]$ (—) indicates the oxidation state of Zn as +2 in both samples. (b) Pd K-edge XANES data collected on $Pd(OAc)_2$ (—), $PdZn(OAc)_4(OH_2)$ (—) and $[(PdZn)_3(btc)_4]$ (—) indicates the oxidation state of Pd as +2 in these three samples, which is compared against that of Pd(0) foil (—).

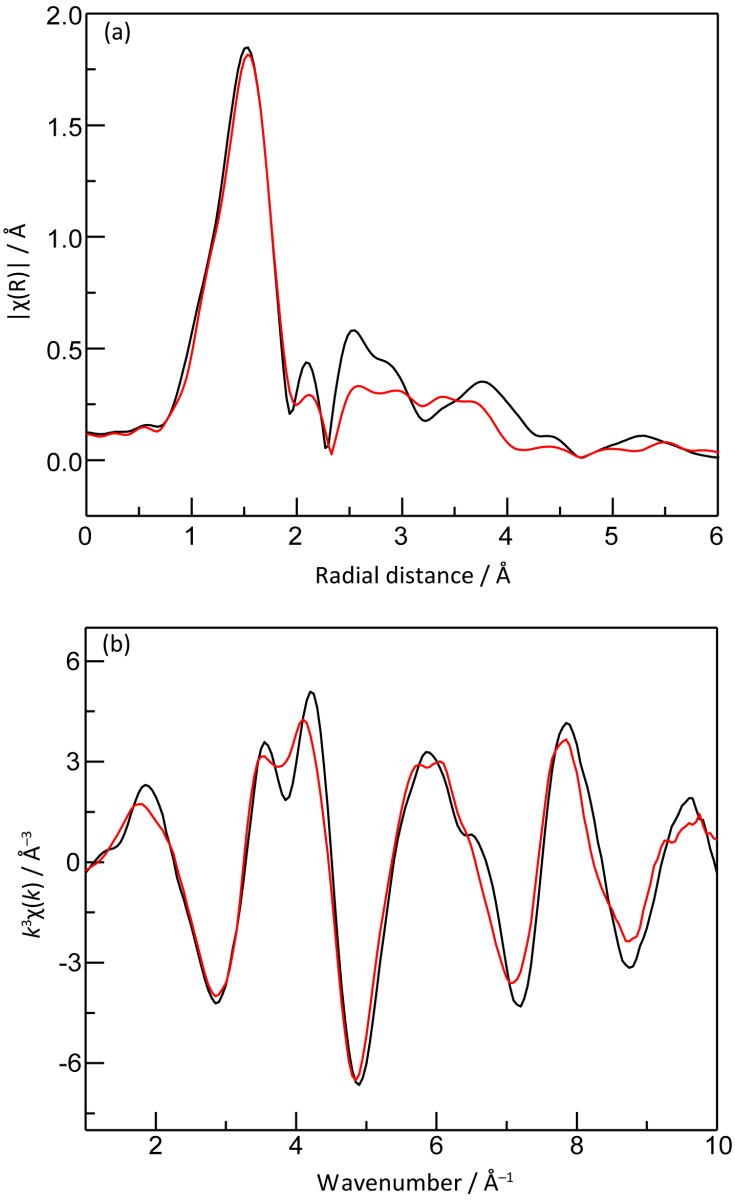

Figure S20. Zn K-edge EXAFS data in *R*-space for $PdZn(OAc)_4(OH_2)$ (—) and $[(PdZn)_3(btc)_4]$ (—). (b) Zn K-edge EXAFS data in *k*-space for $PdZn(OAc)_4(OH_2)$ (—) and $[(PdZn)_3(btc)_4]$ (—). These data highlight that Zn(II) in $PdZn(OAc)_4(OH_2)$ and $[(PdZn)_3(btc)_4]$ shares the same primary coordination sphere and the mechanochemical process does not alternate its primary coordination sphere.

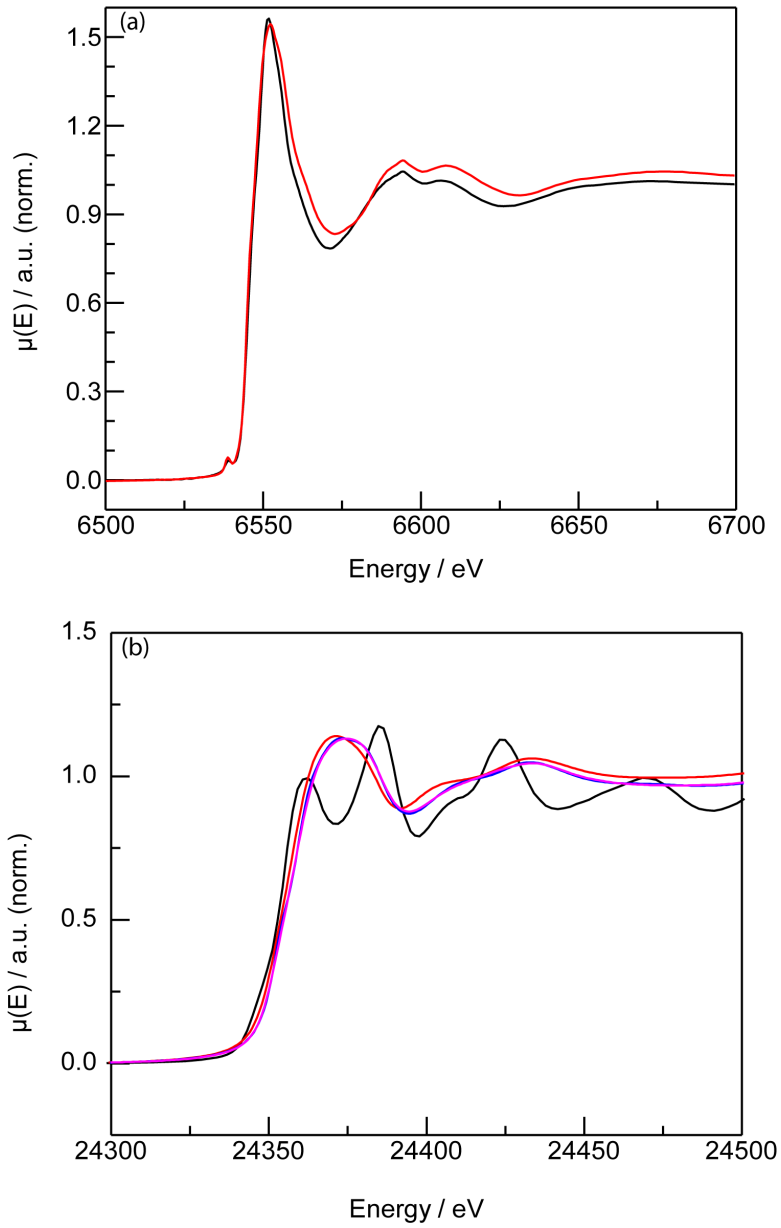

Figure S21. (a) Mn K-edge XANES data collected on for $PdMn(OAc)_4(OH_2)$ (—) and $[(PdMn)_3(btc)_4]$ (—) indicates the oxidation state of Mn as +2 in both samples. (b) Pd K-edge XANES data collected on $Pd(OAc)_2$ (—), $PdMn(OAc)_4(OH_2)$ (—) and $[(PdMn)_3(btc)_4]$ (—) indicates the oxidation state of Pd as +2 in these three samples, which is compared against that of Pd(0) foil (—).

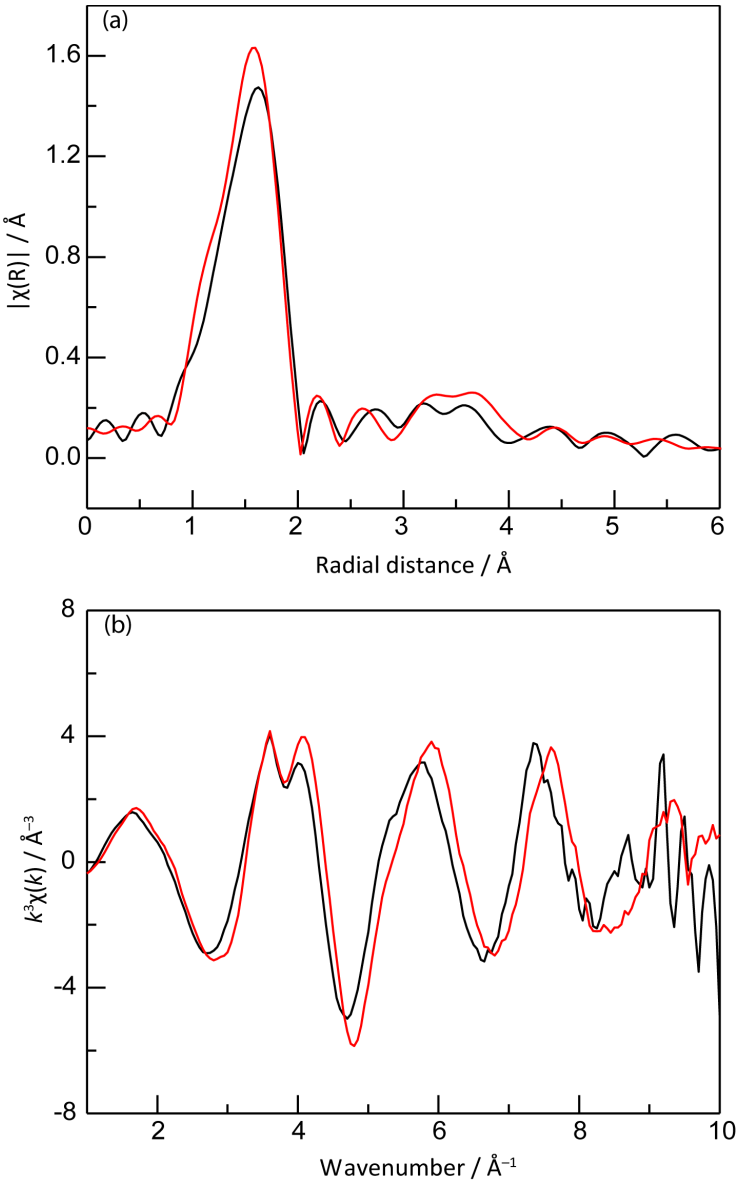

Figure S22. Mn K-edge EXAFS data in *R*-space for $PdMn(OAc)_4(OH_2)$ (—) and $[(PdMn)_3(btc)_4]$ (—). (b) Mn K-edge EXAFS data in *k*-space for $PdMn(OAc)_4(OH_2)$ (—) and $[(PdMn)_3(btc)_4]$ (—). These data highlight that Mn(II) in $PdMn(OAc)_4(OH_2)$ and $[(PdMn)_3(btc)_4]$ shares the same primary coordination sphere and the mechanochemical process does not alternate its primary coordination sphere.

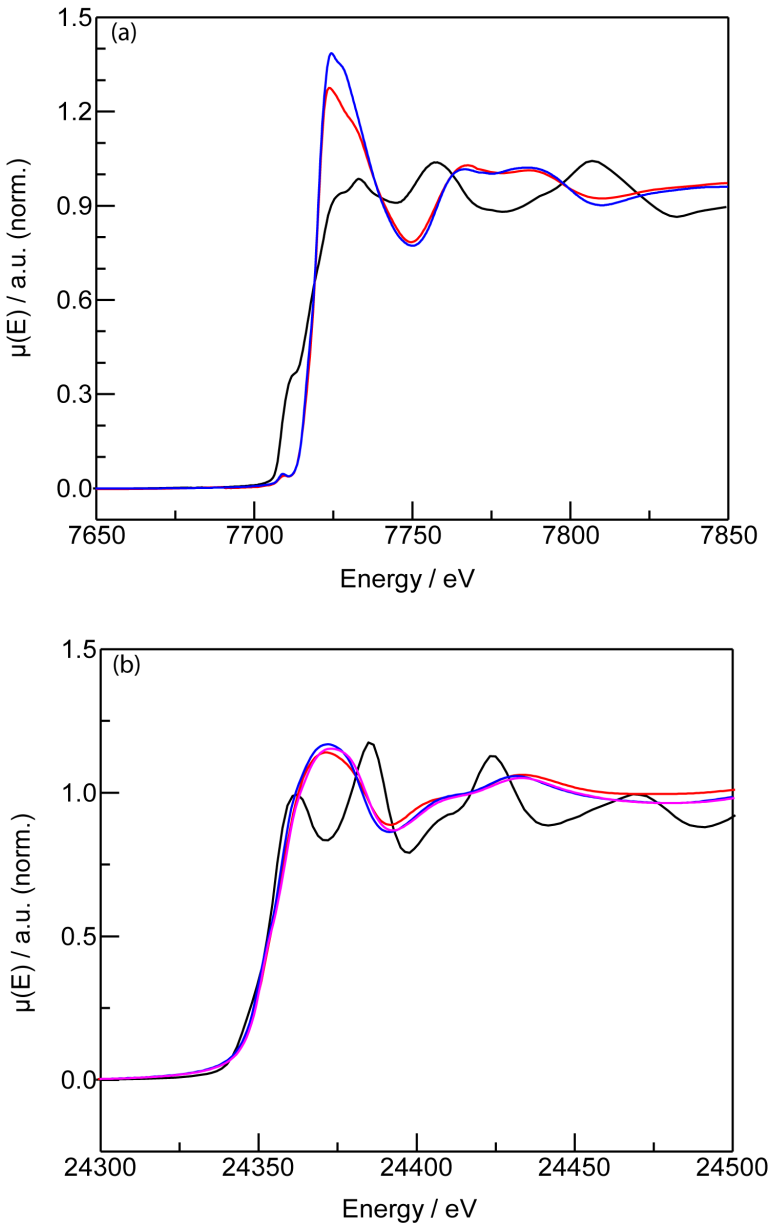

Figure S23. (a) Co K-edge XANES data collected on for $PdCo(OAc)_4(OH_2)$ (—) and $[(PdCo)_3(btc)_4]$ (—) indicates the oxidation state of Co as +2 in both samples, which is compared against Co(0) foil (—). (b) Pd K-edge XANES data collected on $Pd(OAc)_2$ (—), $PdCo(OAc)_4(OH_2)$ (—) and $[(PdCo)_3(btc)_4]$ (—) indicates the oxidation state of Pd as +2 in these three samples, which is compared against that of Pd(0) foil (—).

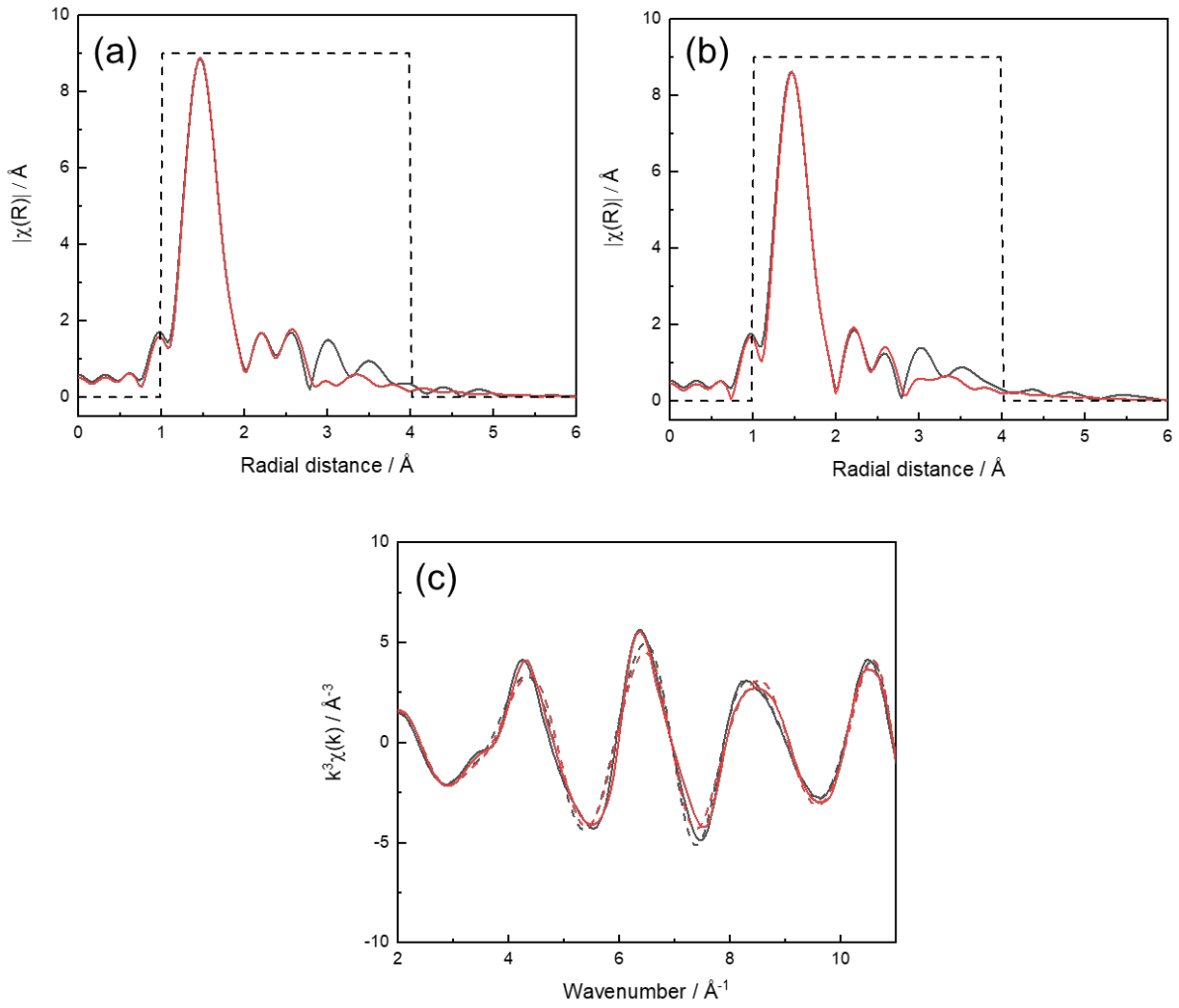

Figure S24. Pd K-edge EXAFS data (fitting range 1.0–4.0 Å) in *R*-space for $PdCo(OAc)_4(OH_2)$ (a) and $[(PdCo)_3(btc)_4]$ (b) (experimental data (—) and fit (—)). (c) Pd K-edge EXAFS data (fitting range 1.0-10.0 $Å^{-1}$) in *k*-space for $PdCo(OAc)_4(OH_2)$ (experimental data (—) and fit (- - -)) and $[(PdCo)_3(btc)_4]$ (experimental data (—) and fit (----)).

Table S5. Pd K-edge EXAFS fitting results of $PdCo(OAc)_4(OH_2)$ and $[(PdCo)_3(btc)_4]$.

	Path	R / Å	CN	σ^2 / Å^2	S_0^2	ΔE / eV	R-Factor
$PdCo(OAc)_4(OH_2)$	Pd-O	1.98(1)	2.0	0.004(1)	0.9 ± 0.1	2.70 ± 1	0.022
	Pd-O	2.13(1)	2.0	0.001(3)			
	Pd-Co	2.50(1)	1.0	0.006(1)			
$[(PdCo)_3(btc)_4]$	Pd-O	2.01(1)	2.0	0.002(2)	0.9 ± 0.1	4.61 ± 1	0.025
	Pd-O	2.17(1)	2.0	0.006(3)			
	Pd-Co	2.53(1)	1.0	0.008(1)			

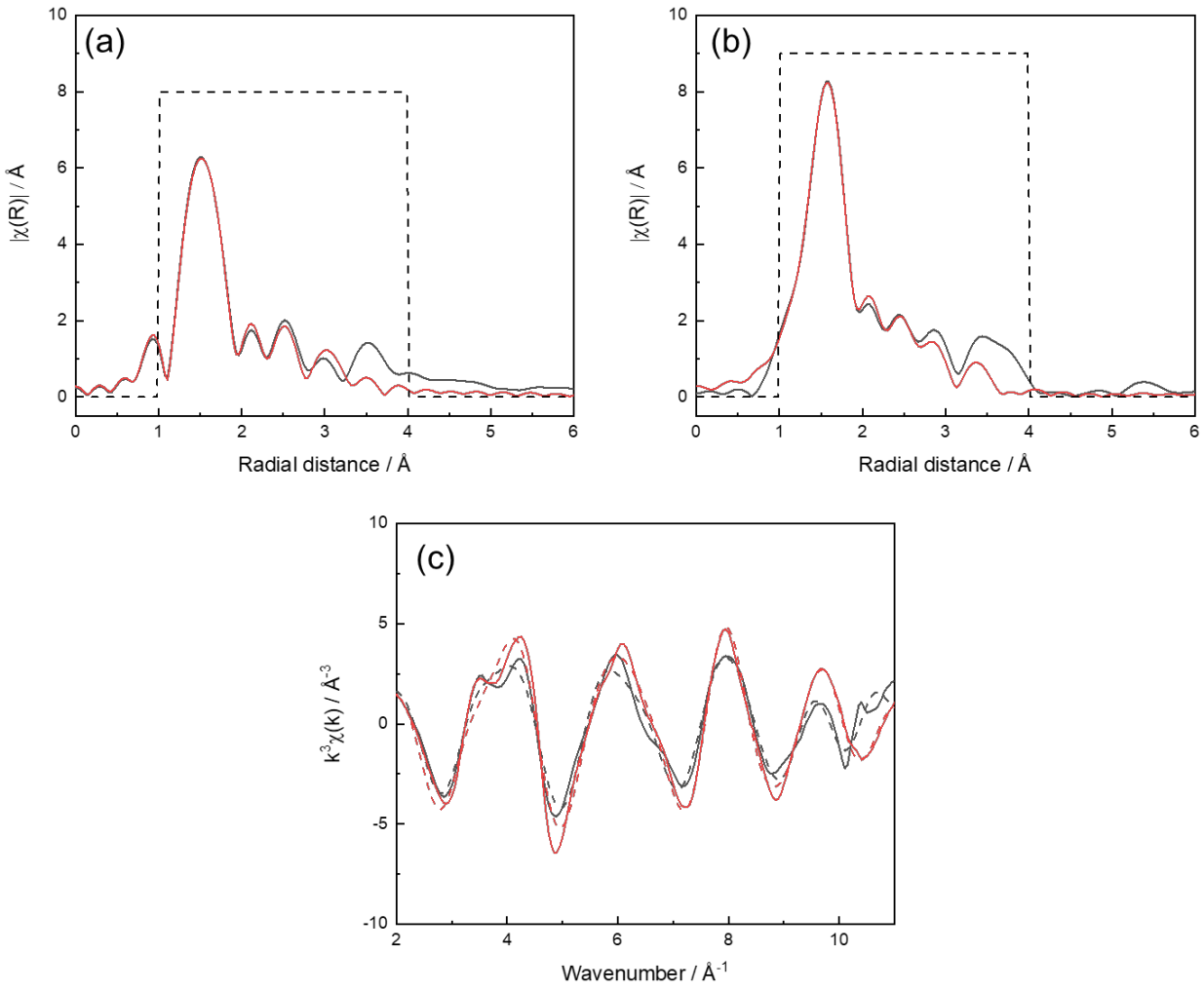

Figure S25. Co K-edge EXAFS data (fitting range 1.0–4.0 Å) in *R*-space for $PdCo(OAc)_4(OH_2)$ (a) and $[(PdCo)_3(btc)_4]$ (b) (experimental data (—) and fit (—)). (c) Co K-edge EXAFS data (fitting range 1.0-10.0 $Å^{-1}$) in *k*-space for $PdCo(OAc)_4(OH_2)$ (experimental data (—) and fit (----)) and $[(PdCo)_3(btc)_4]$ (experimental data (—) and fit (----)).

Table S6. Co K-edge EXAFS fitting results of $PdCo(OAc)_4(OH_2)$ and $[(PdCo)_3(btc)_4]$

	Path	R / Å	CN	σ^2 / Å^2	S_0^2	ΔE / eV	R-Factor
$PdCo(OAc)_4(OH_2)$	Co-O	2.02(1)	2.0	0.004(2)	0.9 ± 0.1	6.94 ± 1	0.032
	Co-O	2.09(1)	2.0	0.006(2)			
	Co-O	2.10(1)	1.0	0.003(1)			
	Co-Pd	2.65(1)	1.0	0.001(1)			
$[(PdCo)_3(btc)_4]$	Co-O	2.03(1)	2.0	0.004(2)	0.9 ± 0.1	6.94 ± 1	0.035
	Co-O	2.10(1)	2.0	0.004(2)			
	Co-O	2.13(1)	1.0	0.006(1)			
	Co-Pd	2.70(1)	1.0	0.003(1)			

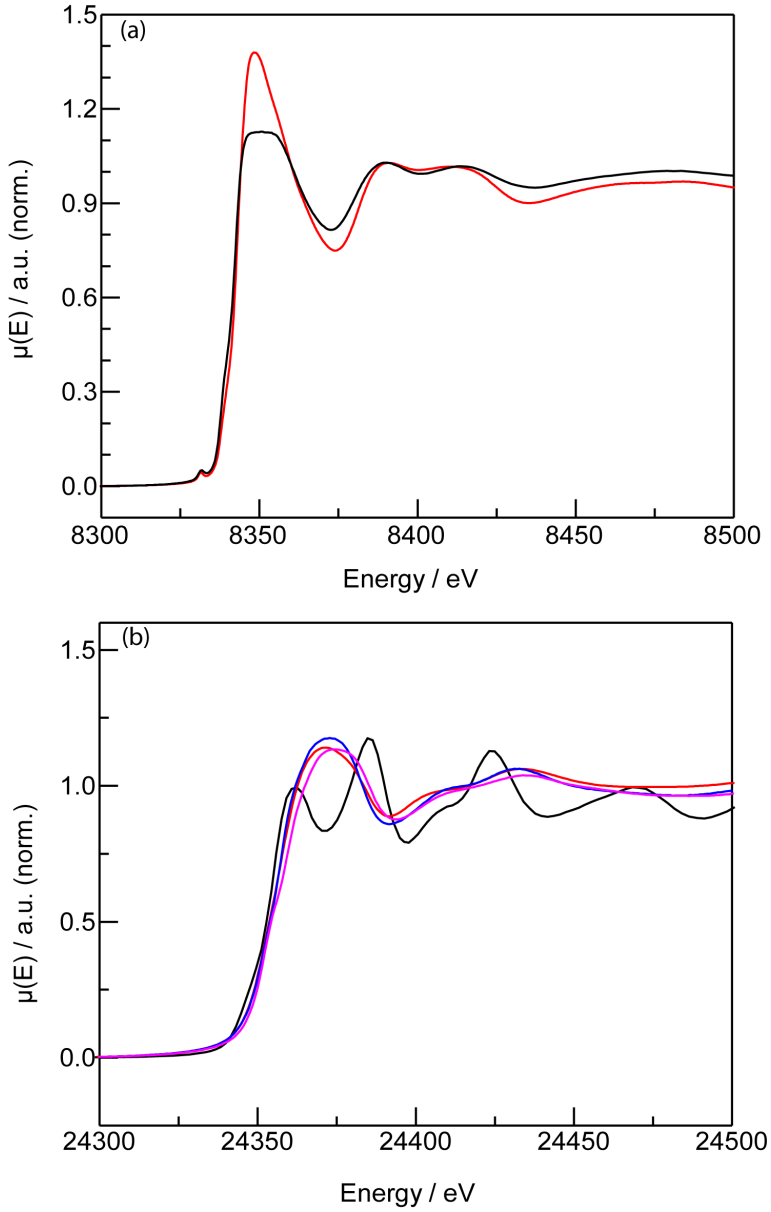

Figure S26. (a) Ni K-edge XANES data collected on for $PdNi(OAc)_4(OH_2)$ (—) and $[(PdNi)_3(btc)_4]$ (—) indicates the oxidation state of Ni as +2 in both samples. (b) Pd K-edge XANES data collected on $Pd(OAc)_2$ (—), $PdNi(OAc)_4(OH_2)$ (—) and $[(PdNi)_3(btc)_4]$ (—) indicates the oxidation state of Pd as +2 in these three samples, which is compared against that of Pd(0) foil (—).

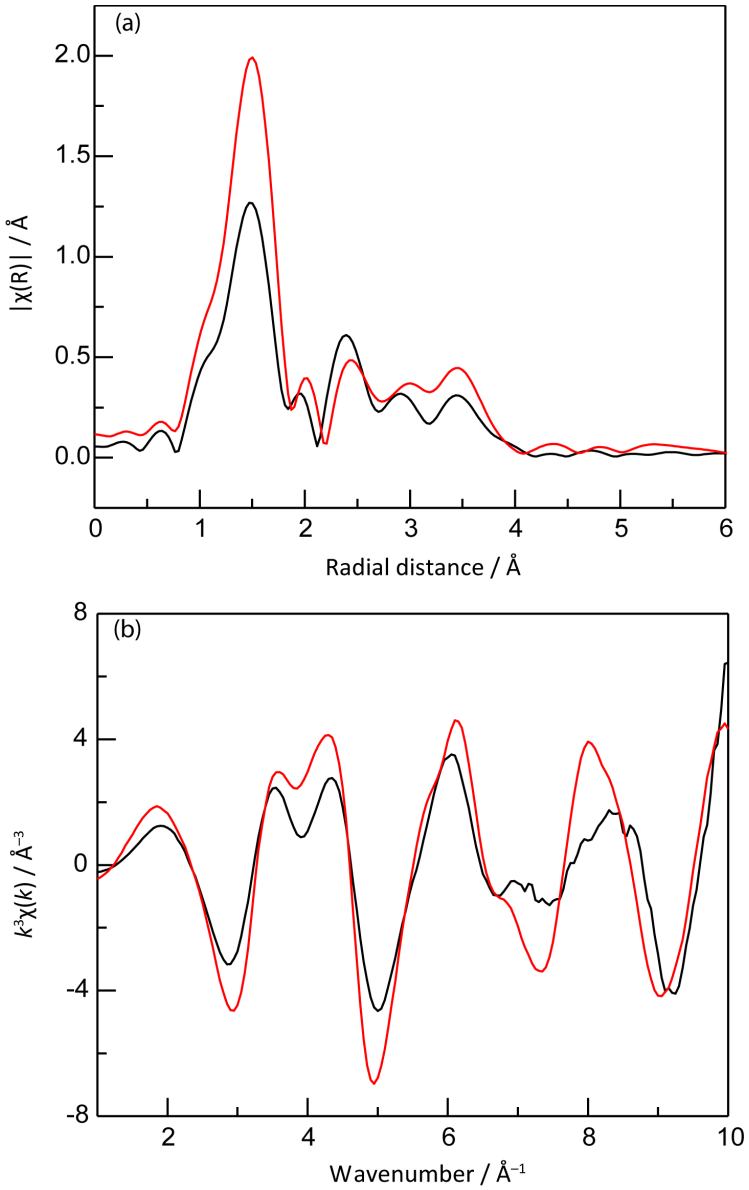

Figure S27. Ni K-edge EXAFS data in *R*-space for $PdNi(OAc)_4(OH_2)$ (—) and $[(PdNi)_3(btc)_4]$ (—). (b) Ni K-edge EXAFS data in *k*-space for $PdNi(OAc)_4(OH_2)$ (—) and $[(PdNi)_3(btc)_4]$ (—). These data highlight that Ni(II) in $PdNi(OAc)_4(OH_2)$ and $[(PdNi)_3(btc)_4]$ shares the same primary coordination sphere and the mechanochemical process does not alternate its primary coordination sphere.

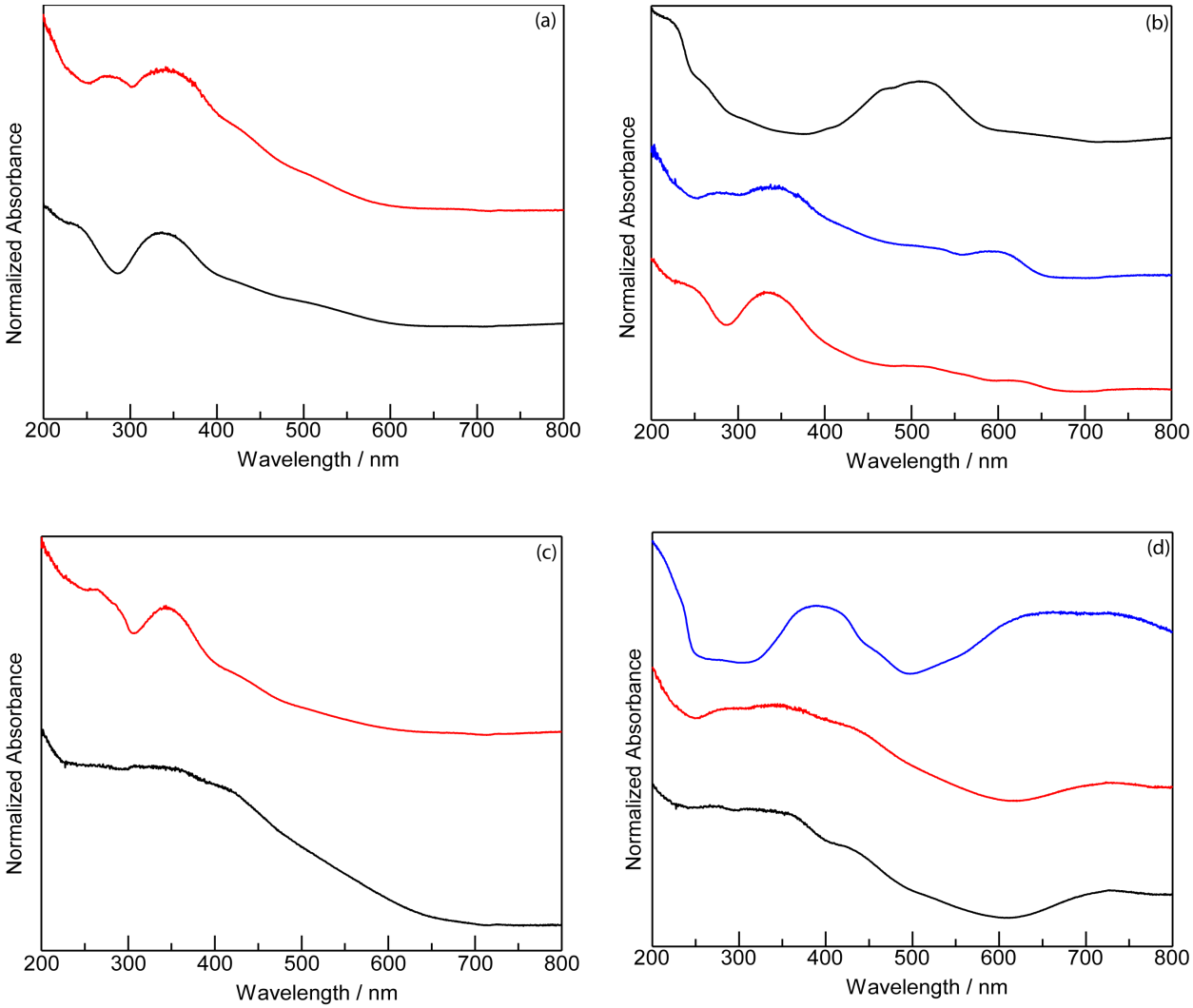

Figure S28. (a) Diffuse reflectance spectra were collected from solid-state $PdZn(OAc)_4$(—) and $[(PdZn)_3(btc)_4]$(—). (b) Diffuse reflectance spectra were collected from solid-state $Co(OAc)_2$(—), $PdCo(OAc)_4$(—) and $[(PdCo)_3(btc)_4]$(—). (c) Diffuse reflectance spectra were collected from solid-state $PdMn(OAc)_4$(—) and $[(PdMn)_3(btc)_4]$(—). (d) Diffuse reflectance spectra were collected from solid-state $Ni(OAc)_2$(—), $PdNi(OAc)_4$(—) and $[(PdNi)_3(btc)_4]$(—). The electronic absorption features sustain from molecular complexes to extended heterobimetallic lattices, which serves as additional evidence for the unchanged heterobimetallic electron configuration through the mechanochemistry.

Table S7. The metal ratio of Pd and M (M = Cu, Zn, Mn, and Co) observed in the mechanochemically prepared multimetallic materials detected by ICP-MS.

Entry	Metal ratio
$[(PdCu)_{1.5}(PdZn)_{1.5}(btc)_4]$	Pd : Cu : Zn = 1 : 0.47 : 0.44
$[[(PdCu)(PdZn)(PdMn)(btc)_4]$	Pd : Cu : Zn : Mn = 1 : 0.30 : 0.31 : 0.34
$[(PdCu)_{0.75}(PdZn)_{0.75}(PdMn)_{0.75}(PdCo)_{0.75}(btc)_4]$	Pd : Cu : Zn : Mn : Co = 1 : 0.21 : 0.22 : 0.25 : 0.29

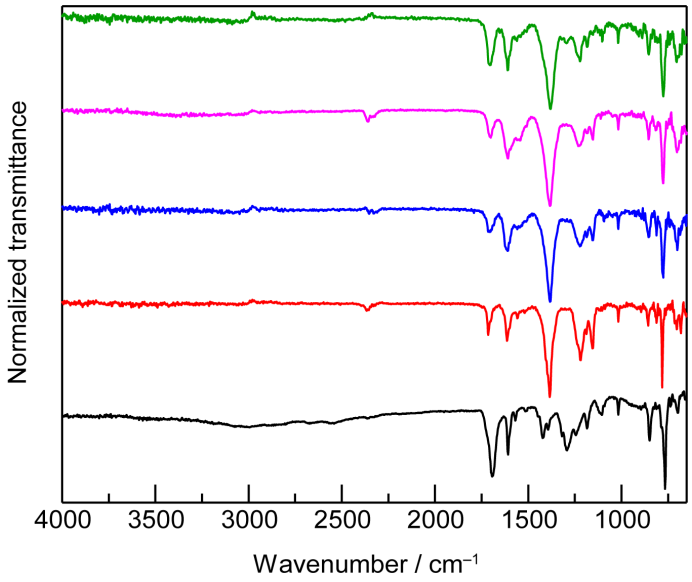

Figure S29. IR spectra (4000–650 cm^{-1}) of H_3btb (—), $[(PdCu)_3(btb)_4]$ (—), $[(PdZn)_3(btb)_4]$ (—), $[(PdMn)_3(btb)_4]$ (—), and $[(PdCo)_3(btb)_4]$ (—). IR provides a diagnostic probe for the reaction progress of mechanochemical synthesis by examining the disappearances of the carbonyl C=O stretch around 1690 cm^{-1} and C–O stretch at 1293 cm^{-1} from initial carboxylic acid.

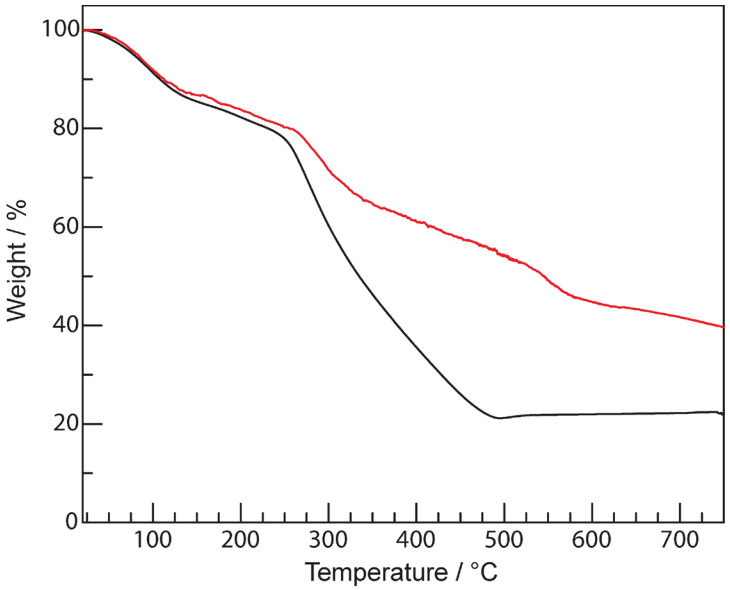

Figure S30. Plots of weight% vs. temperature were obtained by thermogravimetric analysis of $[(PdCu)_3(btb)_4]$ (—) and $[Cu_3(btb)_2]$ (—).

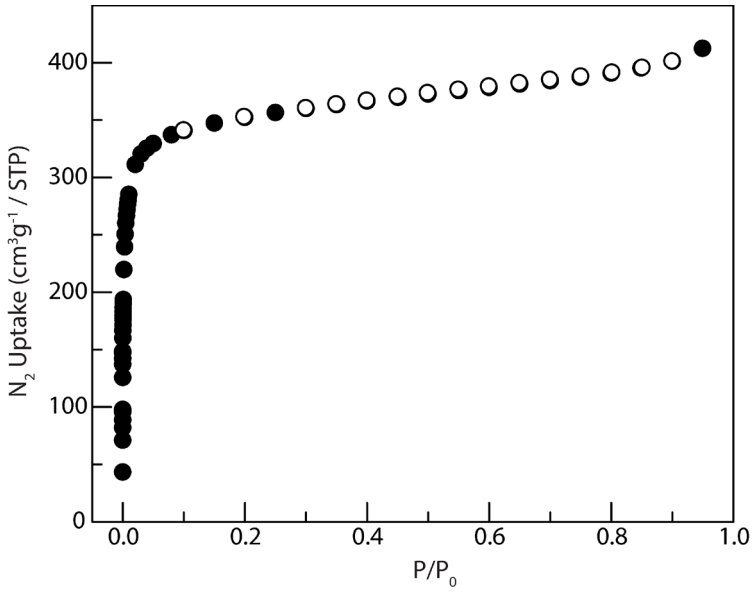

Figure S31. N_2 adsorption isotherm of the mechanochemically synthesized $[(PdCu)_3(btb)_4]$ (adsorption (●), desorption (○)) collected at 77 K. The Brunauer-Emmett-Teller surface area is calculated to 1286 m^2/g (P/P_0 = 0.02–0.15) for $[(PdCu)_3(btb)_4]$.

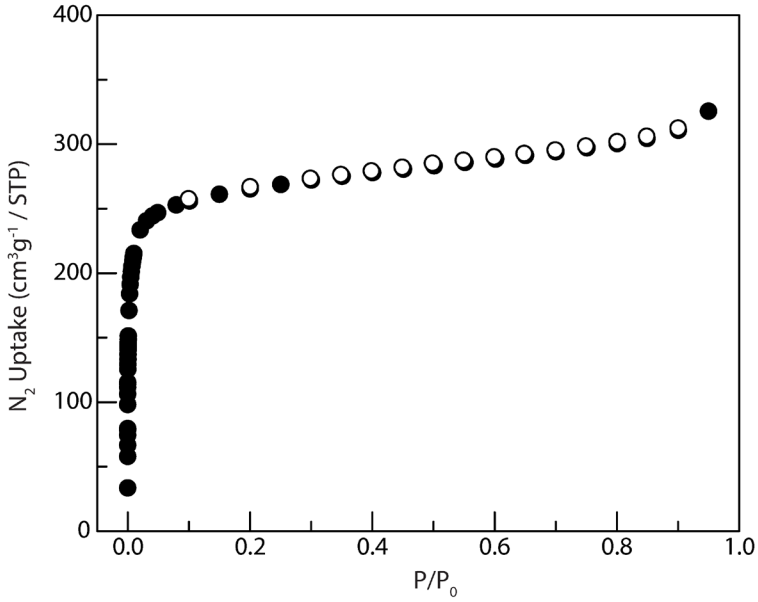

Figure S32. N_2 adsorption isotherm of the mechanochemically synthesized $[(PdCo)_3(btb)_4]$ (adsorption (●), desorption (○)) collected at 77 K. The Brunauer-Emmett-Teller surface area is calculated to 909 m^2/g (P/P_0 = 0.02–0.15) for $[(PdCo)_3(btb)_4]$.

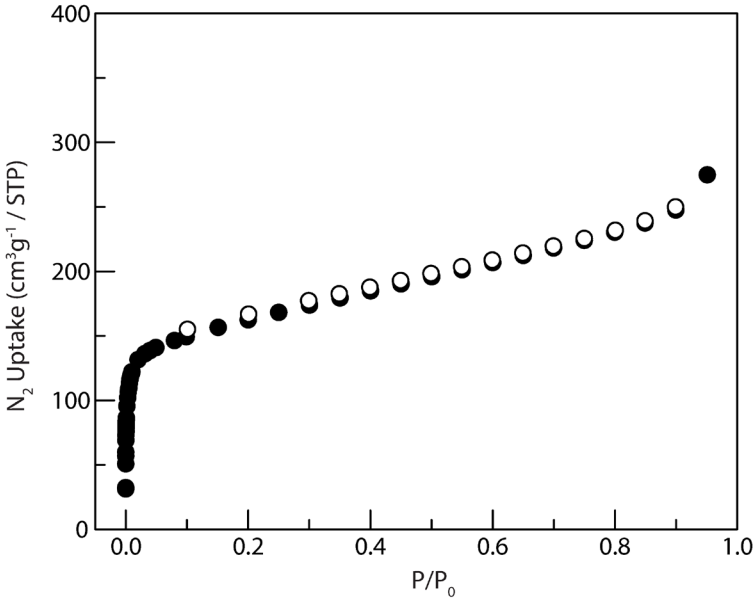

Figure S33. N_2 adsorption isotherm of the mechanochemically synthesized $[(PdMn)_3(btb)_4]$ (adsorption (●), desorption (○)) collected at 77 K. The Brunauer-Emmett-Teller surface area is calculated to 581 m^2/g (P/P_0 = 0.02–0.15) for $[(PdMn)_3(btb)_4]$.

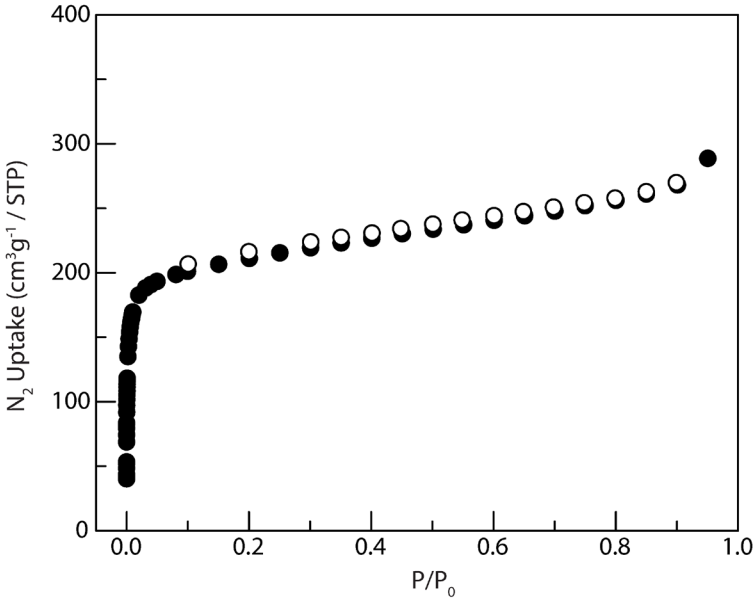

Figure S34. N_2 adsorption isotherm of the mechanochemically synthesized $[(PdZn)_3(btb)_4]$ (adsorption (●), desorption (○)) collected at 77 K. The Brunauer-Emmett-Teller surface area is calculated to 765 m^2/g (P/P_0 = 0.02–0.15) for $[(PdZn)_3(btb)_4]$.

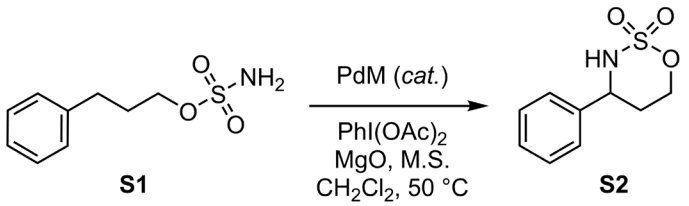

A 4-mL vial was charged with 3-phenylpropyl sulfamate (**S1**, 21.5 mg, 0.100 mmol, 1.00 equiv), $PhI(OAc)_2$ (45.0 mg, 0.140 mmol, 1.40 equiv), CH_2Cl_2 (600 μL), MgO (12.0 mg), molecular sieves (8.1 mg) with 4.0 mol% molecular heterobimetallic complexes or 10 mol% [PdM]-based MOFs for 48 h. The reaction mixtures were heated to 50 °C. Product ratios are reported based on integration of NMR.

Table S8. Summary of the results of intramolecular amination with the molecular catalysts and MOFs. The results demonstrate the relative order of catalyst selectivity depends on the metal identity.

Entry	Catalyst	Mass / mg	Yield (%)
1	$PdCo(OAc)_4$	2.0	44
2	$[(PdCo)_3(btb)_4]$	9.4	32

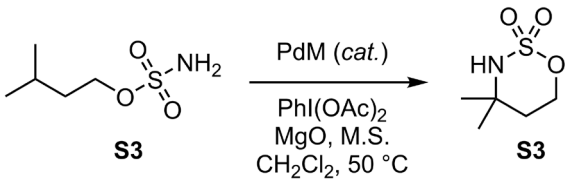

A 4-mL vial was charged with *sopentyl sulfamate* (**S3**, 16.7 mg, 0.100 mmol, 1.00 equiv), $PhI(OAc)_2$ (45.0 mg, 0.140 mmol, 1.40 equiv), CH_2Cl_2 (600 µL), magnesium oxide (MgO, 12 mg), molecular sieves (M.S., 8.1 mg) with 4.0 mol% molecular heterobimetallic complexes or 10 mol% [PdM]-based MOFs for 48 h. The reaction mixtures were heated to 50 °C. Product ratios are reported based on integration of NMR.

Table S9. Summary of the results of intramolecular amination with molecular catalysts and MOFs. The results demonstrate the relative order of catalyst selectivity depends on the metal identity.

Entry	Catalyst	Mass / mg	Yield (%)
1	$PdCo(OAc)_4$	2.0	60
2	$[(PdCo)_3(btb)_4]$	9.4	32

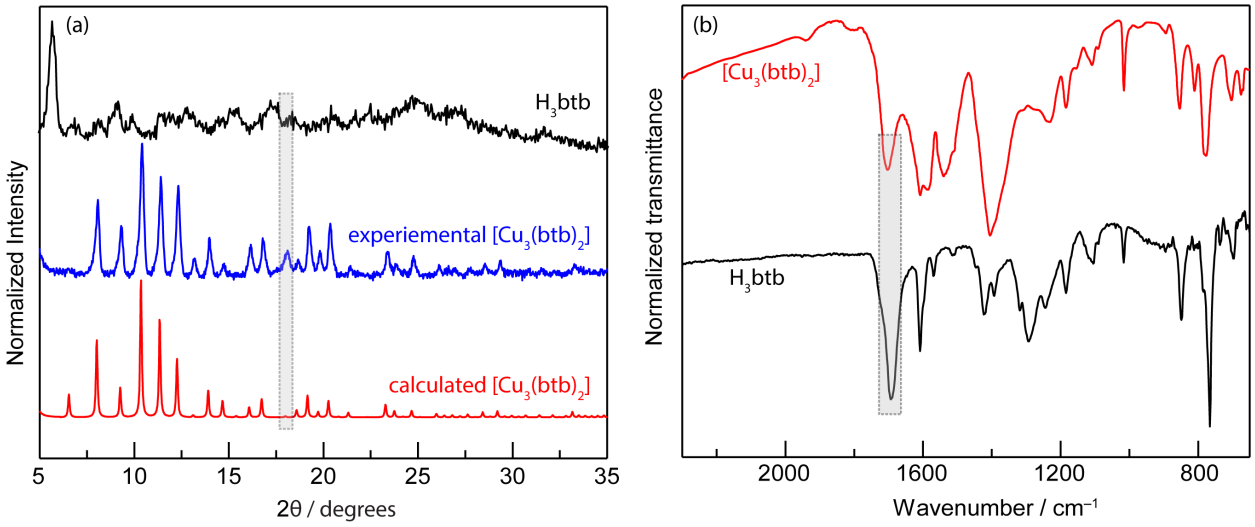

Figure S35. (a) PXRD patterns of the H_3btb ligand (—) and the mechanochemically synthesized $[Cu_3(btb)_2]$ (—) were compared with the calculated patterns (—) of $[Cu_3(btb)_2]$. The notable additional peak at 2θ = 18.1° from $[Cu_3(btb)_2]$ is tentatively attributed to the unreacted H_3btb ligand residue, although the PXRD patterns of the bulk phase H_3btb do not provide a diffraction peak at the same angle. However, this assignment is consistent with the observation from IR data. (b) The IR spectrum of the mechanochemically obtained $[Cu_3(btb)_2]$ indicates that the presence of unreacted carboxylic acid groups possibly from the trapped ligand. Meanwhile, the diffraction peak 2θ = 18.1° was occasionally observed in literature.[8] For instance, the solvothermally prepared $[Cu_3(btb)_2]$ (MOF-14) from Lian et al. also exhibits such a peak.

D. References

1. Harvey, M. E.; Musaev, D. G.; Du Bois, J., A Diruthenium Catalyst for Selective, Intramolecular Allylic C–H Amination: Reaction Development and Mechanistic Insight Gained through Experiment and Theory. *J. Am. Chem. Soc.* **2011,** *133*, 17207-17216.
2. Fiori, K. W.; Espino, C. G.; Brodsky, B. H.; Du Bois, J., A mechanistic analysis of the Rh-catalyzed intramolecular C–H amination reaction. *Tetrahedron* **2009,** *65*, 3042-3051.
3. Toby, B. H.; Von Dreele, R. B., GSAS-II: the genesis of a modern open-source all purpose crystallography software package. *J. Appl. Crystallogr.* **2013,** *46*, 544-549.
4. Macrae, C. F.; Edgington, P. R.; McCabe, P.; Pidcock, E.; Shields, G. P.; Taylor, R.; Towler, M.; van de Streek, J., Mercury: visualization and analysis of crystal structures. *J. Appl. Crystallogr.* **2006,** *39*, 453-457.
5. Ravel, B.; Newville, M., ATHENA, ARTEMIS, HEPHAESTUS: data analysis for X-ray absorption spectroscopy using IFEFFIT. *J. Synchrotron Radiat.* **2005,** *12*, 537-541.
6. Mustre de Leon, J.; Rehr, J. J.; Zabinsky, S. I.; Albers, R. C., Ab initio curved-wave x-ray-absorption fine structure. *Phys. Rev. B* **1991,** *44*, 4146-4156.
7. Akhmadullina, N. S.; Cherkashina, N. V.; Kozitsyna, N. Y.; Stolarov, I. P.; Perova, E. V.; Gekhman, A. E.; Nefedov, S. E.; Vargaftik, M. N.; Moiseev, I. I., Synthesis of palladium(II) 3d-metal(II) paddlewheel acetate-bridged heterodimetallic complexes: Unexpected catalysis by water molecules. *Inorganica Chim. Acta* **2009,** *362*, 1943-1951.
8. Zhao, X.; Xin, C.; Yin, Y.; Tian, X.; Li, Y.; Bian, W.; Lian, P., Metal Organic Framework as an Adsorbent for Desulphurization. *Adsorpt. Sci. Technol.* **2012**, *30*, 483-490.